Targeting the MMP-14/MMP-2/integrin $\alpha_v\beta_3$ axis with multispecific N-TIMP2–based antagonists for cancer therapy

Received for publication, June 10, 2018 Published, Papers in Press, July 9, 2018, DOI 10.1074/jbc.RA118.004406

Gal Yosef, Valeria Arkadash, and Niv Papo[1]

From the Department of Biotechnology Engineering and the National Institute of Biotechnology in the Negev, Ben-Gurion University of the Negev, Beer-Sheva, Israel

Edited by Eric R. Fearon

The pathophysiological functions of the signaling molecules matrix metalloproteinase-14 (MMP-14) and integrin $\alpha_v\beta_3$ in various types of cancer are believed to derive from their collaborative activity in promoting invasion, metastasis, and angiogenesis, as shown *in vitro* and *in vivo*. The two effectors act in concert in a cell-specific manner through the localization of pro-MMP-2 to the cell surface, where it is processed to intermediate and matured MMP-2. The matured MMP-2 product is localized to the cell surface via its binding to integrin $\alpha_v\beta_3$. The MMP-14/MMP-2/integrin $\alpha_v\beta_3$ axis thus constitutes an attractive putative target for therapeutic interventions, but the development of inhibitors that target this axis remains an unfulfilled task. To address the lack of such multitarget inhibitors, we have established a combinatorial approach that is based on flow cytometry screening of a yeast-displayed N-TIMP2 (N-terminal domain variant of tissue inhibitor of metalloproteinase-2) mutant library. On the basis of this screening, we generated protein monomers and a heterodimer that contain monovalent and bivalent binding epitopes to MMP-14 and integrin $\alpha_v\beta_3$. Among these proteins, the bi-specific heterodimer, which bound strongly to both MMP-14 and integrin $\alpha_v\beta_3$, exhibited superior ability to inhibit MMP-2 activation and displayed the highest inhibitory activity in cell-based models of a MMP-14-, MMP-2-, and integrin $\alpha_v\beta_3$-dependent glioblastoma and of endothelial cell invasiveness and endothelial capillary tube formation. These assays enabled us to show the superiority of the combined target effects of the inhibitors and to investigate separately the role each of the three signaling molecules in various malignant processes.

A variety of cancers are believed to stem from the dysregulation of signaling pathways that mediate cell behavior, *i.e.* proliferation, survival, migration, and invasion. Among the signaling molecules that have been implicated in the etiology of different cancers are integrin $\alpha_v\beta_3$ and matrix metalloproteinase-14 (MMP-14, also known as membrane–type-1 matrix metalloproteinase). Integrin $\alpha_v\beta_3$, like all integrins, binds to extracellular matrix (ECM)[2] proteins, thereby promoting cell adhesion to the ECM and activating the signaling pathways involved in the progression of the cell cycle (1) and in angiogenesis (2, 3). MMP-14 is associated with proteolysis, angiogenesis, and cell migration and invasion in the ECM, with elevated levels being correlated with malignancy in different types of cancer (4, 5). In those cancers, it is the catalytic site on the extracellular domain of MMP-14 that drives invasion by enabling MMP-14 to function as a pericellular collagenase (6) and as an activator of pro-MMP-2 (7, 8). A number of studies on a variety of human cancers have shown a correlation between the proteolytic activities of MMP-14 and activated MMP-2, on the one hand, and the extent of endothelial cell invasion, on the other; these studies have also shown a direct link between these two MMPs and pericellular degradation, leading to angiogenesis and metastasis (8–11). For many human tumors, poor prognosis has thus been correlated with the dysregulation and overexpression of integrin $\alpha_v\beta_3$ (12, 13) and MMP-14 and MMP-2 (10), indicating that this axis could constitute an important target for therapeutic intervention.

The concept for designing such a therapeutic intervention may be drawn from numerous papers demonstrating cross-talk between biological processes mediated by MMP-14, integrin $\alpha_v\beta_3$, and their ligands, particularly pathways responsible for angiogenesis (14, 15) and metastasis (16, 17). In addition, recent studies have demonstrated a functional interaction between MMP-14 and integrin $\alpha_v\beta_3$. For example, it is known that integrin $\alpha_v\beta_3$, which is highly expressed on vascular sprouts (endothelial cells) during angiogenesis and on tumor cells (*e.g.* breast cancer, glioblastoma, and melanoma), localizes MMP-14 at the cell migration front (18) and attracts secreted MMP-2 to the cell surface, thereby promoting cell invasiveness (19, 20). In addition, MMP-14 and integrin $\alpha_v\beta_3$ associate on primary endothelial cells and together play a role in endothelial cell migration (18). A cooperative role of MMP-14 and integrin $\alpha_v\beta_3$ in activating pro-MMP-2 has also been reported (21), as has the co-immunoprecipitation of an MMP-14/integrin $\alpha_v\beta_3$/MMP-2 complex from glioma cells (20, 22, 23). Finally, MMP-14 has been shown to participate catalytically in the maturation of the integrin α_v subunit and to correlate with β_3 chain proteolytic cleavage and processing, both of which lead to functional activation of integrin $\alpha_v\beta_3$, thus modulat-

This work was supported by European Research Council "Ideas Program" ERC-2013-StG, Contract Grant 336041, and Israel Science Foundation Grant 615/14 (to N. P.). The authors declare that they have no conflicts of interest with the contents of this article.

This article contains Figs. S1–S7 and Table S1.

[1] To whom correspondence should be addressed. E-mail: papo@bgu.ac.il.

[2] The abbreviations used are: ECM, extracellular matrix; ANOVA, analysis of variance; MMP, matrix metalloproteinase; YSD, yeast surface display; ES, expression sort; TIME, telomerase-immortalized microvascular endothelial; PE, phycoerythrin; SPR, surface plasmon resonance; DMEM, Dulbecco's modified Eagle's medium; FBS, fetal bovine serum; IBB, integrin-binding buffer; Fwd, forward; Rev, reverse; FL, full length.

ing the adhesive, migratory, and metastatic behavior of tumor cells (23, 24).

MMP-14 and integrin $\alpha_v\beta_3$ work in concert to facilitate the processing and maturation of MMP-2 (21). This maturation is initiated by activation of pro-MMP-2 into intermediate MMP-2 in a process that is facilitated by two molecules of MMP-14 and one molecule of FL-TIMP2, the full-length molecule of tissue inhibitor of metalloproteinases 2 (TIMP2). Through its N-terminal domain, FL-TIMP2 binds to the catalytic site of one MMP-14 molecule, leading to MMP-14 inhibition. Through its C-terminal domain, cell-surface localized FL-TIMP2 binds to pro-MMP-2, thereby bringing it into the proximity of a second (catalytically active) MMP-14 molecule, which processes pro-MMP-2 into the MMP-2 intermediate form (21, 25, 26). Conversion of the intermediate MMP-2 into matured MMP-2 takes place in an integrin $\alpha_v\beta_3$-dependent process, but the details of this specific maturation mechanism remain to be elucidated (21, 23). It is the latter two forms of MMP-2 (*i.e.* intermediate and matured) that are able to degrade ECM components and to promote invasiveness (27, 28). Importantly, although MMP-2 is a secreted protein, localization of matured MMP-2 on cancer and endothelial cell surfaces, via integrin $\alpha_v\beta_3$, was found to increase cell invasiveness and angiogenesis (19, 29).

Given the complexity and redundancy of the MMP-14, MMP-2, and integrin $\alpha_v\beta_3$ signaling networks that result from the cross-talk between these effectors, it is likely that multicomponent therapeutics capable of perturbing parallel nodes of these critical pathways that are associated with angiogenesis and metastasis would be a promising means to combat drug resistance in various cancers, including melanoma (22), glioma (20), and breast cancer (21). Indeed, such a notion has attracted considerable attention for other systems and has accelerated the development of mixture therapeutics targeted at other cross-reactive signaling networks, such as vascular endothelial growth factor– epidermal growth factor receptor inhibitors (30, 31), many of which have already been introduced into pre-clinical and clinical practice (30). Nonetheless, despite their significant clinical success, mixture therapeutics have several well known limitations, including additive on- and off-target toxicity (32, 33). Moreover, their use is limited by the requirement to provide preclinical data demonstrating that the mixture has greater than additive activity or more durable responses than those obtained with mono-therapy (34). These limitations may be overcome by exploiting the enormous potential of combinatorial approaches for engineering multispecificity into natural protein ligands (35–37).

In this paper, we demonstrate that concurrent targeting of MMP-14 and integrin $\alpha_v\beta_3$ with bi-specific inhibitors offers enhanced therapeutic benefits compared with the respective mono-treatments. We show that these bi-specific inhibitors are the first reported proteins that target all the known functions that result from cross-talk between MMP-14 and integrin $\alpha_v\beta_3$, namely cancer cell invasion, angiogenesis, and MMP-2 activation and localization to the cell surface. The bi-specific inhibitors were derived from the 127-amino acid N-terminal domain of WT TIMP-2 (N-TIMP2$_{WT}$) and that of an N-TIMP2 variant, designated N-TIMP2$_{5M}$, which was previously designed by our group for high affinity and specificity toward MMP-14 in preference to other MMPs (38). An overriding consideration in the design of the above inhibitors was the need for specificity, because MMP family members are also found in nonmalignant cells, and some MMPs, such as MMP-8 and MMP-12, exhibit anti-tumorigenic functions (39–41). It is thus not surprising that inhibitors with narrow or single MMP specificity have greater therapeutic potential than nonspecific inhibitors (42–44). As we have shown previously, specificity toward MMP-14 in preference to other MMPs can be obtained by utilizing N-TIMP2$_{5M}$ (38), but cell specificity can best be achieved by tailoring the inhibitors for binding specificity to both MMP-14 and its co-localized receptor integrin $\alpha_v\beta_3$.

One of the main challenges that we had to address was engineering specificity for integrin $\alpha_v\beta_3$ binding, because the Arg-Gly-Asp (RGD) tripeptide motif typical of many natural ECM ligands, including fibronectin, vitronectin, fibrinogen, and osteopontin, is also recognized by other integrins, including those containing the α_v subunit and integrins $\alpha_5\beta_1$ and $\alpha_{iib}\beta_3$ (45). To generate mutated N-TIMP2 variants with binding specificity toward integrin $\alpha_v\beta_3$, we exploited the substantial differences between the above ligands in the three-dimensional orientations of flexible solvent-exposed loops containing the RGD motif; these differences are a function of the particular amino acid residues flanking the RGD sequence and hence dictate the integrin-binding affinity and specificity of the ligands (46).

N-TIMP2 shows extensive sequence diversity both within and between species (47), as its exposed loops are highly tolerant to substitution or to incorporation of additional amino acids (38, 47–49). To achieve high target affinity and specificity, we exploited these attributes of N-TIMP2 for use as a versatile platform for the development of both bivalent single-domain and heterodimeric MMP-14/integrin $\alpha_v\beta_3$ inhibitors that were generated from affinity high-throughput screens of an N-TIMP2$_{RGD}$–loop library with random amino acid changes. The engineered bi-specific proteins were expressed as soluble proteins and were shown to bind simultaneously to both MMP-14 and integrin $\alpha_v\beta_3$, with different inhibitory and antagonistic activities, both *in vitro* and in cells. The bi-specific monomeric and heterodimeric inhibitors displayed superior therapeutic potential to that of MMP-14 and integrin $\alpha_v\beta_3$ mono-treatments. In addition, the availability of both mono- and bi-specific proteins allowed us to dissect out the role of each target in cell invasion and angiogenesis and to design inhibitors with superior potencies for each of these two cancerous processes, separately and together.

Results

N-TIMP2$_{RGD}$ loop library construction and screening

An N-TIMP2$_{RGD}$ yeast surface display (YSD) loop library was designed in such a way that positions 51–59 at the apex of loop B–C in N-TIMP2, which naturally binds integrin $\alpha_3\beta_1$, were replaced with a sequence comprising an RGD motif flanked on each side by three additional random amino acids (*XXX*RGD*XXX*) (Fig. 1*A* and Fig. S1). To isolate high-affinity bi-specific N-TIMP2 binders for the MMP-14 catalytic domain

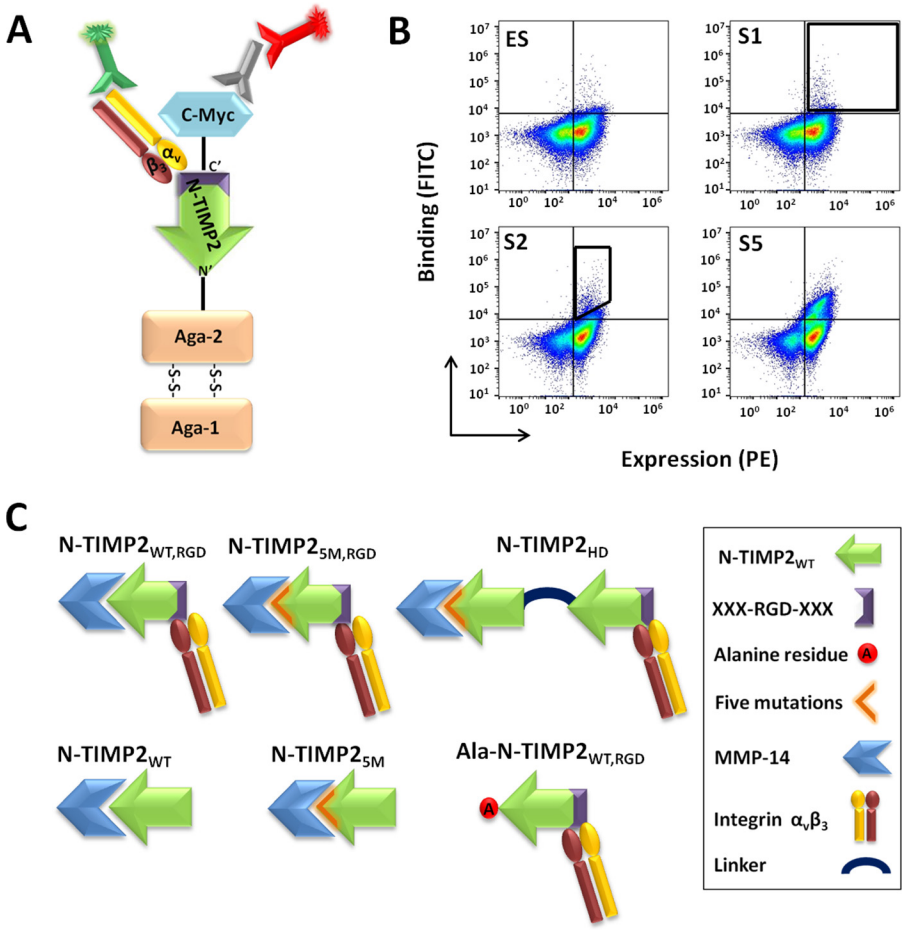

Figure 1. Strategy for screening the N-TIMP2$_{RGD}$ library. *A,* YSD system. N-TIMP2$_{RGD}$ proteins were displayed on yeast. Expression of the N-TIMP2$_{RGD}$ proteins was detected by targeting the c-Myc epitope tag, expressed at the C terminus of the protein, with an antibody labeled with PE, and binding to integrin $\alpha_v\beta_3$ was detected by FITC staining. *B,* flow cytometry analysis of the sorted library tested against 50 nM integrin $\alpha_v\beta_3$. In the expression sort (ES), the entire N-TIMP2$_{RGD}$ protein–expressing cell population was sorted (black gate). In sort 1 (*S1*), the yeast cell population binding to integrin $\alpha_v\beta_3$ was collected (black gate). In sort 2 (*S2*) to sort 5 (*S5*), the integrin $\alpha_v\beta_3$ high-affinity population was collected (black gate). The population binding integrin $\alpha_v\beta_3$ was enriched as the sorting progressed from S2 to S5. *C,* N-TIMP2 protein variants. N-TIMP2$_{WT, RGD}$ is the bi-specific protein isolated after sort 5. N-TIMP2$_{5M, RGD}$ is N-TIMP2$_{WT, RGD}$ with five mutations (5M); this mutant showed improved binding to MMP-14 (38). N-TIMP2$_{HD}$ is a heterodimer composed of N-TIMP2$_{5M}$ and N-TIMP2$_{WT, RGD}$ proteins conjugated via a peptide linker. N-TIMP2$_{WT}$ and N-TIMP2$_{5M}$ are mono-specific binders for MMP-14. Ala–N-TIMP2$_{WT, RGD}$ has a reduced affinity toward MMP-14 and a high affinity toward integrin $\alpha_v\beta_3$.

(MMP-14$_{CAT}$, residues 112–292) (50) and integrin $\alpha_v\beta_3$, six rounds of flow-cytometry sorting were performed, the first one for high-expressing clones (expression sort, ES) and the other five (sorts 1–5) for binding to soluble integrin $\alpha_v\beta_3$ (Fig. 1, *A* and *B*). In each round of sorting (sorts 1–5), the concentration of integrin $\alpha_v\beta_3$ was reduced, and the cell population binding integrin $\alpha_v\beta_3$ was enriched (Fig. 1*B*). Nine different clones were identified after sort 5 (Table 1). One of the nine clones, namely clone 2, designated N-TIMP2$_{WT, RGD}$ (Fig. S2), was chosen for further purification as a soluble protein on the basis of its strong integrin $\alpha_v\beta_3$ binding. This clone was then purified as a free N-terminal protein (which is crucial for MMP inhibition; Fig. S3), having a His tag and a c-Myc tag, both at the C terminus of the protein.

N-TIMP2 variants exhibit different affinities toward MMP-14 and integrin $\alpha_v\beta_3$

To optimize the inhibitory activity of the N-TIMP2 variants and to dissect out the contribution of each target receptor to tumor progression, we generated a pool of N-TIMP2 variants with different affinities for each target. We have recently shown that insertion of five point mutations, namely I35M, N38D, S68N, V71G, and H97R, into N-TIMP2 (generating N-TIMP2$_{5M}$) increases its affinity toward MMP-14 by 890-fold (38). In this study, we therefore incorporated these mutations into the bi-specific monomer, N-TIMP2$_{WT, RGD}$, thereby generating the N-TIMP2$_{5M, RGD}$ variant (Fig. 1*C*). We also engineered Ala–N-TIMP2$_{WT, RGD}$, a protein variant having high affinity toward integrin $\alpha_v\beta_3$ and reduced inhibition activity toward MMP-14, by inserting an alanine residue before the cysteine residue at position 1 (Fig. 1*C*). We note that alanine insertion in TIMP2 was previously shown to abolish binding to MMP and its inhibition (51). N-TIMP2$_{WT}$ and N-TIMP2$_{5M}$ served as mono-specific binders with different affinities to MMP-14 but no affinity to integrin $\alpha_v\beta_3$. In addition, an N-TIMP2 heterodimer (N-TIMP2$_{HD}$), composed of N-TIMP2$_{5M}$ at the N terminus fused via a flexible peptidic linker to N-TIMP2$_{WT, RGD}$ at the C terminus, was designed so as to reduce the mutual effects of the N-TIMP2$_{5M}$ and N-TIMP2$_{WT, RGD}$ mutations on each other's activity.

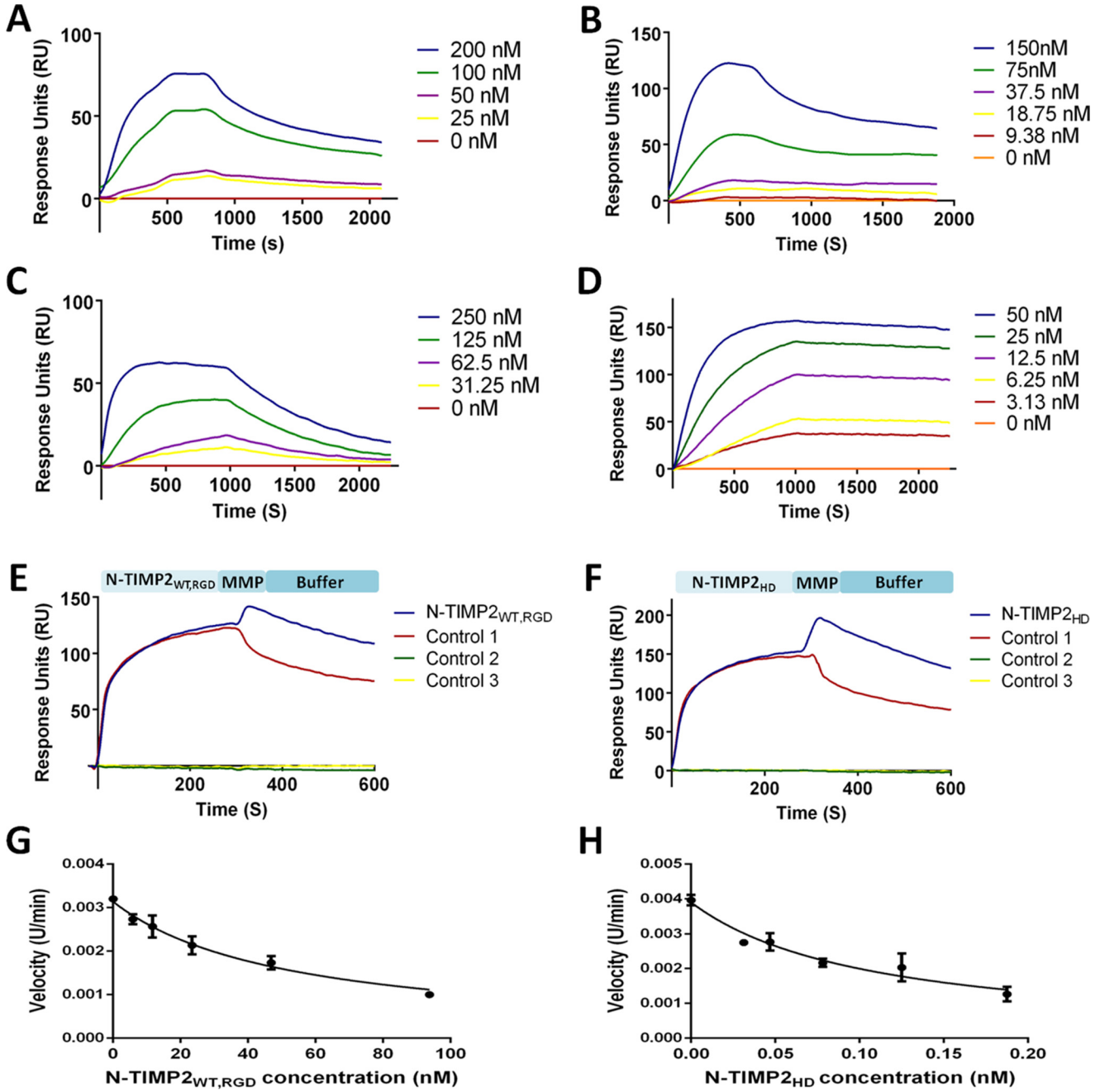

Figure 2. SPR sensorgrams and the inhibitory activity of the N-TIMP2$_{WT, RGD}$ and N-TIMP2$_{HD}$ variants. N-TIMP2$_{WT, RGD}$ (*A*) and N-TIMP2$_{HD}$ (*B*) binding to integrin $\alpha_v\beta_3$ is shown. N-TIMP2$_{WT, RGD}$ (*C*) and N-TIMP2$_{HD}$ (*D*) binding to MMP-14$_{CAT}$ is shown. Dual binding of N-TIMP2$_{WT, RGD}$ (*E*) and N-TIMP2$_{HD}$ (*F*) to integrin $\alpha_v\beta_3$ and MMP-14$_{CAT}$ is shown. *E* and *F*, variants were allowed to flow over integrin $\alpha_v\beta_3$ immobilized on the chip, followed by MMP-14$_{CAT}$ (*blue*) or buffer (control 1, *red*) injection at 300 s. There was an increase in response units (*RU*) for the variants after MMP-14$_{CAT}$ injection, which indicates that these variants bind simultaneously to both receptors. In control 2 (*green*), a buffer was allowed to flow over the integrin $\alpha_v\beta_3$ immobilized chip, followed by MMP-14 injection at 300 s. In control 3 (*yellow*), a buffer was allowed to flow over the integrin $\alpha_v\beta_3$ immobilized chip throughout the entire experiment. Substrate degradation velocity at different concentrations of N-TIMP2$_{WT, RGD}$ (0–100 nM) (*G*) and N-TIMP2$_{HD}$ (0–0.2 nM) (*H*) were fitted to Morrison's equation (Equation 2) to obtain K_i values.

The bi-specific monomer N-TIMP2$_{WT, RGD}$ was shown to bind both integrin $\alpha_v\beta_3$ and MMP-14$_{CAT}$, with K_D values of 64.8 nM (Fig. 2*A*) and 838 nM (Fig. 2*C*), respectively (Table 1). Moreover, N-TIMP2$_{WT, RGD}$ was capable of binding both receptors simultaneously, as determined by a co-injection surface plasmon resonance (SPR) assay (Fig. 2*E*). We have previously shown that the insertion of the five mutations into N-TIMP2$_{5M}$ improved the affinity to MMP-14$_{CAT}$ compared with N-TIMP2$_{WT}$ (38). As expected, binding to integrin $\alpha_v\beta_3$ was not detected for the TIMP2$_{WT}$ and N-TIMP2$_{5M}$ monospecific MMP-14 variants (Fig. S4*A*). In agreement with these results, the insertion of the five mutations into N-TIMP2$_{5M, RGD}$ significantly increased the affinity toward MMP-14$_{CAT}$ by ~400-fold (K_D of 2 nM), although the affinity toward integrin $\alpha_v\beta_3$ was decreased (K_D of 531 nM) but not completely abolished (Table 1 and Fig. S4, *C* and *D*). The results of a comparison of the K_D values obtained for the two monomeric bi-specific binders, N-TIMP2$_{WT, RGD}$ and

Table 1
Binding kinetics of N-TIMP2 variants
ND means binding not detected at 1 μM concentration; NA means not available; NT means not tested.

N-TIMP2 variant	MMP-14 kinetics				Integrin $\alpha_v\beta_3$ kinetics		
	K_i	K_D	K_{on}	K_{off}	K_D	K_{on}	K_{off}
	nM	nM	$10^4\ ms^{-1}$	$10^{-5}\ s^{-1}$	nM	$10^4\ ms^{-1}$	$10^{-3}\ s^{-1}$
N-TIMP2$_{WT}$	2.01 ± 0.2	4.68 ± 0.01	11.4	53.6	ND		
N-TIMP2$_{5M}$	0.011 ± 0.003	0.603 ± 0.001[a]	6.2	3.74	ND		
N-TIMP2$_{WT, RGD}$	35.76 ± 2.28	838 ± 12.7	NA	NA	64.8 ± 0.46	1.71 ± 0.01	1.11 ± 0.01
Ala–N-TIMP2$_{WT, RGD}$	132.6 ± 8.55	NT			197 ± 1.1	4.71 ± 0.08	9.28 ± 0.35
N-TIMP2$_{5M, RGD}$	[b]	2.08 ± 0.02	8.39 ± 0.21	17.4 ± 0.13	561 ± 276	NA	NA
N-TIMP2$_{HD}$	0.077 ± 0.023	0.78 ± 0.01	7.6 ± 0.12	5.97 ± 0.09	130 ± 21.1	NA	NA

[a] Data were taken from Arkadash *et al.* (38).
[b] K_i values could not be determined accurately. Complete inhibition was detected at 0.8 nM.

N-TIMP2$_{5M, RGD}$, for both integrin $\alpha_v\beta_3$ and MMP-14$_{CAT}$ implied that by increasing the affinity to one target, the affinity to the other is reduced. However, by separating the two binding domains of each monomer in the engineered bi-specific heterodimer (N-TIMP2$_{HD}$), we were able to generate a protein that had high affinity to both integrin $\alpha_v\beta_3$ and MMP-14$_{CAT}$ (K_D of 130 and 0.78 nM, respectively, see Table 1 and Fig. 2, *B* and *D*). Similarly to N-TIMP2$_{WT, RGD}$, N-TIMP2$_{HD}$ was able to bind both receptors simultaneously, as determined by a co-injection SPR assay (Fig. 2*F*).

In agreement with the SPR binding results, the ability of the N-TIMP2 variants to inhibit MMP-14$_{CAT}$ catalytic activity, as reflected by the K_i values, was as follows (best to worst): N-TIMP2$_{5M}$, N-TIMP2$_{HD}$, N-TIMP2$_{WT}$, N-TIMP2$_{WT, RGD}$, and Ala–N-TIMP2$_{WT, RGD}$ (Table 1). Ala–N-TIMP2$_{WT, RGD}$ showed low inhibitory activity toward MMP-14$_{CAT}$, although it retained its ability to bind to integrin $\alpha_v\beta_3$ (Table 1 and Fig. S4*B*).

In summary, three important points emerge from these results. 1) The three engineered bi-specific proteins bind to both targets but with different affinities: N-TIMP2$_{WT, RGD}$ binds strongly to integrin $\alpha_v\beta_3$ but weakly to MMP-14; N-TIMP2$_{5M, RGD}$ binds strongly to MMP-14 but weakly to integrin $\alpha_v\beta_3$; and N-TIMP2$_{HD}$ binds strongly to both receptors. 2) N-TIMP2$_{WT, RGD}$ and N-TIMP2$_{HD}$ can bind simultaneously to both receptors. 3) There was good correlation between the K_D (SPR) and K_i (inhibition of MMP-14 catalytic activity) potencies.

N-TIMP2 variants inhibit MMP-2 activation in the U87MG cell line

A major outcome of the cross-talk between MMP-14 and integrin $\alpha_v\beta_3$ is the processing/maturation of pro-MMP-2 to intermediate and subsequently fully matured MMP-2 forms. The MMP-2 processing/maturation mechanism takes place in two consecutive steps. In the first step, processing of the 68-kDa pro-MMP-2 by MMP-14 into the 64-kDa MMP-2 intermediate form is followed by conversion of the MMP-2 intermediate form to the matured 62-kDa MMP-2 form. In the second, more rapid, step, it is the interaction of the intermediate MMP-2 with integrin $\alpha_v\beta_3$ that facilitates, via an as-yet-unknown mechanism, the autocatalytic processing of the intermediate MMP-2 to the fully matured MMP-2 (21). Because MMP-2, MMP-14, and integrin $\alpha_v\beta_3$ work in concert, it is not a trivial task to separate out the specific and overall contributions of the intermediate and matured forms of MMP-2 to cancer cell invasion and angiogenesis (52). To address this problem, we evaluated the ability of the mono-specific (inhibiting MMP-14 or integrin $\alpha_v\beta_3$) *versus* the bi-specific (inhibiting both proteins) N-TIMP2 variants to inhibit the activation (maturation process) of MMP-2. For this purpose, we used a gelatin zymography assay, because all MMP-2 forms can cleave gelatin (53), but only the intermediate and the matured species can degrade the ECM components, such as collagen, gelatin, and fibronectin (53, 54), and promote cell invasion, with the matured form being more potent than the intermediate form (55).We utilized two controls for this assay as follows: (i) recombinant FL-TIMP2, a protein that is endogenously expressed in U87MG glioblastoma cells and is known to induce the formation of the matured MMP-2 and cell invasion (56), and (ii) cyclic RGD (cRGD), a known inhibitor of integrin $\alpha_v\beta_3$ (57). In this assay, U87MG cells (expressing both MMP-14 and integrin $\alpha_v\beta_3$, Fig. S5) were treated with 100 nM of each protein variant for 48 h. The culture supernatant, which contained the secreted pro/intermediate/matured MMP-2 forms, was loaded onto a gelatin gel, and the different MMP-2 forms were eluted as white bands on the gel. In addition, different concentrations of FL-TIMP2 and cRGD were tested for their pro-MMP-2 activation function. All the strong inhibitors of MMP-14, namely N-TIMP2$_{WT}$, FL-TIMP2, N-TIMP2$_{5M}$, N-TIMP2$_{5M, RGD}$, and N-TIMP2$_{HD}$, significantly inhibited the processing of endogenous pro-MMP-2 to the intermediate form (Fig. 3, *A* and *B*). However, FL-TIMP2, when added at a lower concentration (10 nM), activated processing of the pro-MMP-2 to the active forms (Fig. S6). Importantly, exposure to Ala–N-TIMP2$_{WT, RGD}$, which binds strongly to integrin $\alpha_v\beta_3$ and possesses a lower MMP-14 inhibition potency, significantly increased the amount of the intermediate MMP-2 form by inhibiting its processing to the matured form; the same was true for cRGD at a concentration of 1 μM (Fig. S7). Thus, whereas Ala–N-TIMP2$_{WT, RGD}$ did not reduce the total amount of the ECM-reactive MMP-2 forms (*i.e.* both intermediate and matured forms that are able to degrade the ECM component) relative to the untreated control, it did increase the ratio between the intermediate (less ECM reactive) product and the matured product. Although N-TIMP2$_{WT, RGD}$ did not significantly inhibit the processing of the intermediate MMP-2, it did exhibit the same tendency to inhibit intermediate MMP-2 processing as the Ala–N-TIMP2$_{WT, RGD}$ variant, with the ratios between

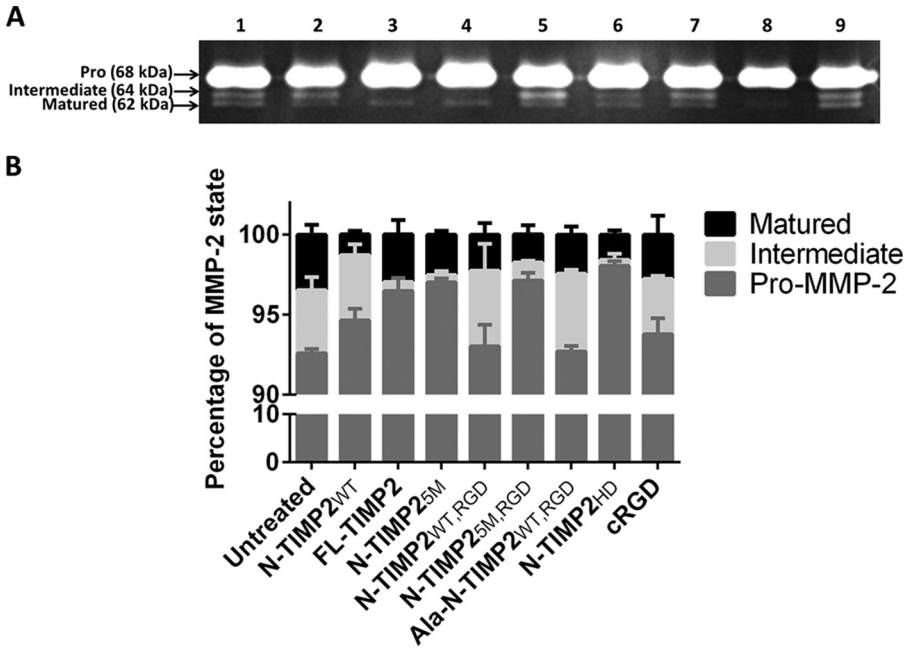

Figure 3. Inhibition of pro-MMP-2 activation by N-TIMP2 variants. *A,* gelatin zymography gel results. The U87MG supernatant was loaded on gelatin zymography gel. *Lane 1* represents untreated U87MG cells, and *lanes 2–8*, respectively, represent treatment with 100 nM of the following N-TIMP2 variants: N-TIMP2$_{WT}$; FL-TIMP2; N-TIMP2$_{5M}$; N-TIMP2$_{WT, RGD}$; N-TIMP2$_{5M, RGD}$; Ala–N-TIMP2$_{WT, RGD}$; and N-TIMP2$_{HD}$. *Lane 9* represents treatment with cRGD (100 nM). *B,* quantification of the percentage of each MMP-2 form, *i.e.* pro/intermediate/matured (band intensity of each MMP-2 state, *i.e.* pro-MMP-2 (68 kDa), intermediate MMP-2 (64 kDa), and matured MMP-2 (62 kDa), was divided by the total band intensity of all the MMP-2 forms). *Error bars* represent S.E. Pro-MMP-2 processing and the total amount of the catalytically active MMP-2 were significantly inhibited by N-TIMP2$_{WT}$ ($p < 0.05$), FL-TIMP2 ($p < 0.01$), and N-TIMP$_{5M}$, N-TIMP2$_{5M, RGD}$, and N-TIMP2$_{HD}$ ($p < 0.001$). Processing of the intermediate form was significantly inhibited by Ala–N-TIMP2$_{WT, RGD}$ ($p < 0.05$). The amount of the matured form of MMP-2 was significantly reduced by N-TIMP2$_{5M}$ and N-TIMP2$_{5M, RGD}$ ($p < 0.05$), N-TIMP2$_{HD}$ ($p < 0.01$), and N-TIMP2$_{WT}$ ($p < 0.001$). Statistical analysis was performed by Student's *t* test compared with the untreated control; $n = 3$.

the intermediate and matured forms of MMP-2 being 2.1 and 2, for N-TIMP2$_{WT, RGD}$ and Ala–N-TIMP2$_{WT, RGD}$, respectively, compared with 1.1 for the untreated control. Because the intermediate MMP-2 form is less ECM-reactive than the fully matured form, it was to be expected that the increase in the intermediate/matured MMP-2 ratio would be reflected in reduced ECM degradation and decreased invasion, as will indeed be shown in this paper. Among all the variants, N-TIMP2$_{HD}$ exhibited the strongest inhibition effect on MMP-2 activation, giving the largest decrease in both the intermediate and the matured forms relative to the other variants.

MMP-2 docking on the U87MG cell surface is impaired by an integrin $\alpha_v\beta_3$ inhibitor

The catalytic activity of MMP-2 localized on the cell surface via integrin $\alpha_v\beta_3$ mediation is known to promote cell invasiveness and angiogenesis (19, 23, 29). We therefore tested the ability of our inhibitors to prevent the interaction between matured MMP-2 and integrin $\alpha_v\beta_3$. Because the SPR results indicated that our bi-specific proteins can simultaneously engage MMP-14 and integrin $\alpha_v\beta_3$, Ala–N-TIMP2$_{WT, RGD}$ (which binds strongly to integrin $\alpha_v\beta_3$ and has low MMP-14 inhibition activity) was selected as the variant to compete with MMP-2 for binding to membrane-anchored integrin $\alpha_v\beta_3$. In keeping with our expectations that the competitive binding would inhibit MMP-2–induced ECM degradation (19), flow cytometry showed that there was indeed a reduction of recombinant matured MMP-2 levels on the surface of the U87MG cells 2 h after treatment with 2 μM Ala–N-TIMP2$_{WT,}$ RGD (67% reduction, Fig. 4*A*). To confirm that the matured form of MMP-2 was indeed removed by Ala–N-TIMP2$_{WT, RGD}$, gelatin zymography was performed on the U87MG cell lysate, which contained the cell-surface–bound MMP-2; it was indeed found that only matured MMP-2 was removed from the cell surface (Fig. 4, *B–D*). To determine whether Ala–N-TIMP2$_{WT, RGD}$ prevents matured MMP-2 binding specifically to integrin $\alpha_v\beta_3$, a solid-phase assay was performed. Purified recombinant integrin $\alpha_v\beta_3$ was immobilized on a 96-well ELISA plate, followed by overnight incubation with either Ala–N-TIMP2$_{WT, RGD}$ or cRGD (2 μM) and with a U87MG supernatant obtained after 48 h of growth, *i.e.* containing all the MMP-2 forms. Both Ala–N-TIMP2$_{WT, RGD}$ and cRGD reduced the docking levels of pro-MMP-2 on integrin $\alpha_v\beta_3$ to a similar extent (~57%, Fig. 4, *E* and *F*), whereas Ala–N-TIMP2$_{WT, RGD}$ significantly inhibited the interaction of matured MMP-2 with integrin $\alpha_v\beta_3$ compared with cRGD treatment (66 and 42%, respectively, Fig. 4, *E* and *G*). The differences between the assay results can be explained by the fact that in the flow cytometry (Fig. 4*A*) recombinant matured MMP-2 was used, whereas in the zymography assays (Fig. 4, *B–G*) all the MMP-2 forms secreted from U87MG cells were present; among all these forms, matured MMP-2 constitutes only <5% (Fig. 3). Because the matured form binds integrin $\alpha_v\beta_3$, greater inhibition of MMP-2 cell-surface localization was observed in Fig. 4*A* compared with Fig. 4, *B–G*. In addition, Fig. 4, *B–D*, presents an assay performed on a U87MG cell lysate, which probably contains other binding receptors for

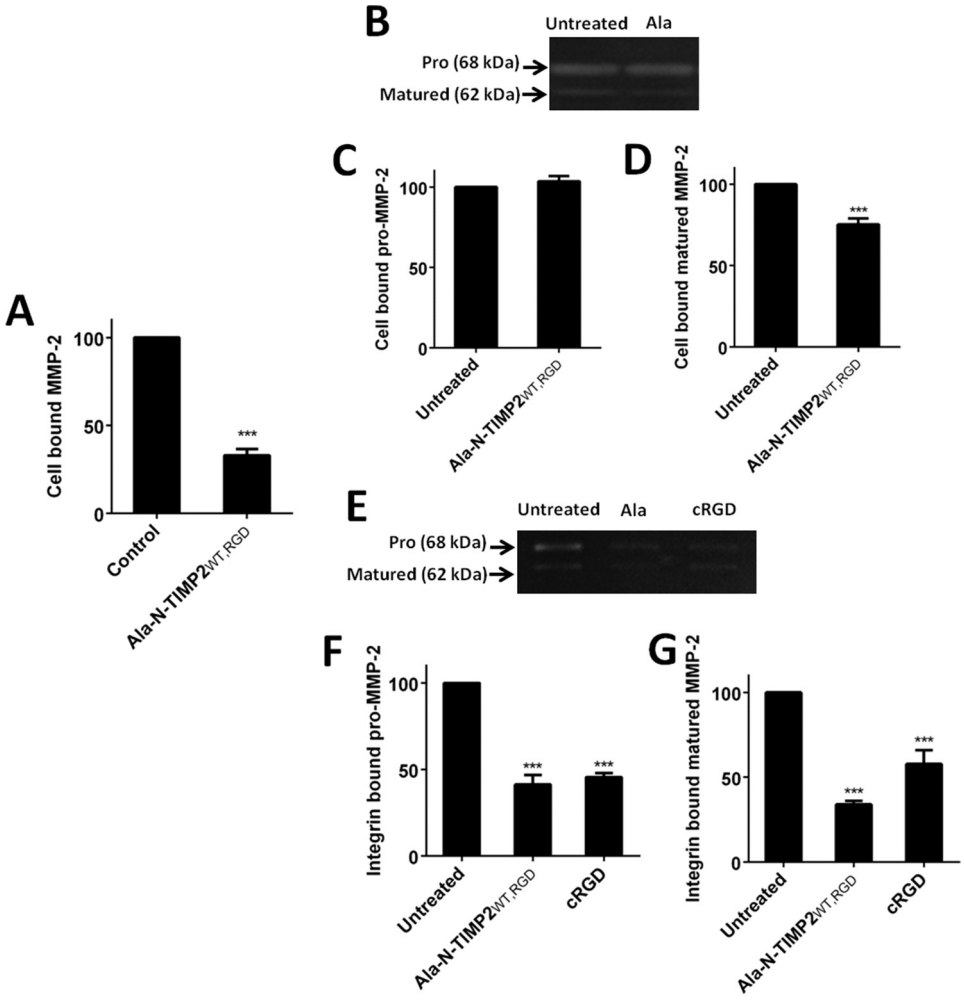

Figure 4. The Ala–N-TIMP2$_{WT,\ RGD}$ variant disrupts matured MMP-2 cell-surface localization by binding to integrin $\alpha_v\beta_3$. *A,* Ala–N-TIMP2$_{WT,\ RGD}$ removes matured MMP-2 from the U87MG cell surface as detected by flow cytometry analysis. A specific antibody against MMP-2 (clone CA-4001, Abcam) was utilized to detect MMP-2 on the U87MG cell surface. *B,* cell lysate gelatin zymography gel of untreated cells (*left*) and 2 μM treatment of Ala–N-TIMP2$_{WT,\ RGD}$ (Ala, *right*). *C,* Ala–N-TIMP2$_{WT,\ RGD}$ does not affect pro-MMP-2 localization on the cell surface. *D,* Ala–N-TIMP2$_{WT,\ RGD}$ removes matured MMP-2 from the cell surface. *E,* integrin $\alpha_v\beta_3$– bound MMP-2 gelatin zymography gel of untreated cells and 2 μM treatment of Ala–N-TIMP2$_{WT,\ RGD}$ and cRGD. *F* and *G,* Ala–N-TIMP2$_{WT,\ RGD}$ and cRGD interfere with binding of pro-MMP-2 (*F*) and matured MMP-2 (*G*) to integrin $\alpha_v\beta_3$. The results were normalized to untreated cells. *Error bars* represent S.D. Statistical analysis was performed by Student's *t* test compared with the untreated control; ***, $p < 0.0001$, $n = 3$.

MMP-2, whereas Fig. 4, *E–G*, shows an assay performed solely on the immobilized recombinant integrin $\alpha_v\beta_3$ receptor. Pro-MMP-2 can bind to other receptors on the cell surface, such as MMP-14 and lipoprotein receptor-related protein-2 (58), and therefore might not be affected by the binding of Ala–N-TIMP2$_{WT,\ RGD}$ to integrin $\alpha_v\beta_3$. For this reason, only a small reduction was observed in Fig. 4, *C* and *D* (several integrins and MMP-14 being present), *versus* Fig. 4, *F* and *G* (integrin $\alpha_v\beta_3$ alone). Moreover, as mentioned previously, it is known that the form of MMP-2 that binds integrin $\alpha_v\beta_3$ is the mature form and not the pro-MMP-2 form. In Fig. 4, *E–G*, only integrin $\alpha_v\beta_3$ was present as a receptor in the system. Thus, there were no alternative receptors with which pro-MMP-2 could interact. Furthermore, whereas pro-MMP-2 was the dominant form of secreted MMP-2 (~95%, Fig. 3), its binding to immobilized integrin $\alpha_v\beta_3$ was slightly higher than that of the mature form, which comprised less than 5% of the secreted MMP-2 forms. The above data thus attest to the preference in binding affinity of integrin $\alpha_v\beta_3$ for matured MMP-2 over pro-MMP-2.

N-TIMP2 variants inhibit the invasion of U87MG cells

Because the invasiveness of cancer cells is influenced by the proteolytic activity of MMP-14 and by integrin $\alpha_v\beta_3$–mediated cell migration, the ability of the N-TIMP2 variants to inhibit the invasion of U87MG cells was evaluated in a Boyden chamber Matrigel® invasion assay (Fig. 5). In this assay, only the heterodimer, N-TIMP2$_{HD}$, and the mixture of N-TIMP2$_{5M}$ and Ala–N-TIMP2$_{WT,\ RGD}$ (Fig. 5, *H, J* and *K*) significantly inhibited the invasion of U87MG cells compared with untreated cells (Fig. 5, *A* and *K*), with the bi-specific N-TIMP2$_{HD}$ heterodimer exhibiting the strongest inhibition effect (33% inhibition, Fig. 5, *H* and *K*). When U87MG cells were treated with a mixture of N-TIMP2$_{5M}$ and Ala–N-TIMP2$_{WT,\ RGD}$, high inhibition activity was observed (26% inhibition, Fig. 5, *I* and *K*), although this inhibition activity was inferior to that of N-TIMP2$_{HD}$, as shown in Fig. 5. This superior inhibitory activity of N-TIMP2$_{HD}$ over the mixture of N-TIMP2$_{5M}$ and Ala–N-TIMP2$_{WT,\ RGD}$ was statistically significant when the comparison was performed

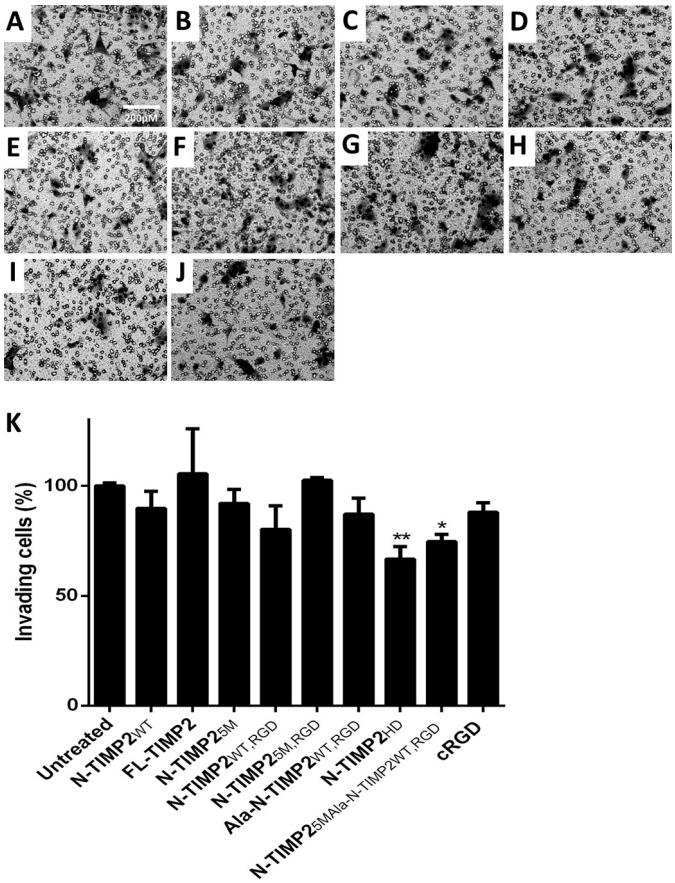

Figure 5. Inhibition of invasion of U87MG cells by N-TIMP2 variants. *A,* untreated cells. Cells were treated with the following: N-TIMP2$_{WT}$ (*B*); FL-TIMP2 (*C*); N-TIMP2$_{5M}$ (*D*); N-TIMP2$_{WT, RGD}$ (*E*); N-TIMP2$_{5M, RGD}$ (*F*); Ala–N-TIMP2$_{WT, RGD}$ (*G*); N-TIMP2$_{HD}$ (*H*); N-TIMP2$_{5M}$ and Ala–N-TIMP2$_{WT, RGD}$ (*I*), and cRGD (*J*). *K,* quantification of invasive cells normalized to untreated cells. *Error bars* represent S.D. One-way ANOVA with Dunnett's multiple comparison with the untreated control was utilized for statistical analysis; *, $p < 0.05$; **, $p < 0.005$, $n = 3$. A comparison between treatment with N-TIMP2$_{HD}$ *versus* all other treatments showed the statistically significant superior inhibition ability of N-TIMP2$_{HD}$ when compared with N-TIMP2$_{WT}$, FL-TIMP2, and Ala–N-TIMP2$_{WT, RGD}$ ($p < 0.05$), N-TIMP2$_{5M}$ and cRGD ($p < 0.005$), and N-TIMP2$_{5M, RGD}$ ($p < 0.001$).

with untreated cells. However, when the two treatments were compared with one another, no statistically significant difference was observed ($p = 0.1089$). Compared with Ala–N-TIMP2$_{WT, RGD}$ (Fig. 5*G*) and N-TIMP2$_{5M}$ (Fig. 5*D*), each alone, N-TIMP2$_{HD}$ exhibited a significantly stronger inhibition effect (Fig. 5*K*), a finding that implies a synergistic inhibition effect between N-TIMP2$_{5M}$ and Ala–N-TIMP2$_{WT, RGD}$. This synergistic inhibition was also observed for the TIME cell line (Fig. 7, *D*, *G*, *H*, and *J*).

N-TIMP2 variants inhibit in vitro angiogenesis in the TIME cell line

Endothelial cells form capillary-like structures when embedded in a Matrigel® matrix. This process, which simulates angiogenesis, involves endothelial cell migration, proliferation, and survival (59). Therefore, N-TIMP2 variants were evaluated for their ability to inhibit tube formation of TIME cells. Although FL-TIMP2 exhibited pro-angiogenic activity (Fig. 6, *C*, *I*, and *J*) and N-TIMP2$_{5M}$ did not demonstrate any effect on angiogenesis (Fig. 6, *D*, *I*, and *J*) as compared with untreated cells (Fig. 6*A*), the other N-TIMP2 variants showed significant inhibition ability (Fig. 6, *B* and *D–H*). Compared with N-TIMP2$_{WT}$, which exhibits good anti-angiogenic activity (61% reduction in of the number of tube segments (Fig. 6, *B* and *I*) and 22% reduction in tube total length (Fig. 6*J*)), the strong integrin $\alpha_v\beta_3$ binders N-TIMP2$_{WT, RGD}$ (82 and 35%, Fig. 6*E*), Ala–N-TIMP2$_{WT, RGD}$ (92 and 56%, Fig. 6*G*), and N-TIMP2$_{HD}$ (79 and 41%, Fig. 6*H*), exhibited a more pronounced inhibition effect. Moreover, whereas both N-TIMP2$_{RGD}$ variants and N-TIMP2$_{WT}$ did affect tube formation, at least in one parameter, *i.e.* tube total length or number of tube segments, cRGD (2 and 50 μM treatments) had no effect on tube formation (data not shown). In contrast to the strong MMP-14 inhibitor N-TIMP2$_{5M}$, N-TIMP2$_{WT}$, although having lower inhibition activity, exhibited strong inhibition of tube formation in TIME cells, a function that may not be related to MMP-14 inhibition but rather to its ability to activate integrin $\alpha_3\beta_1$, previously shown to lead to inhibition of angiogenesis (60). Because specificity to integrin $\alpha_v\beta_3$ compared with other integrins was not tested, it should be noted that inhibition of tube formation might also be mediated by other RGD-binding integrins or integrin $\alpha_3\beta_1$. Notably, the strong inhibition of tube formation seen for the strong integrin $\alpha_v\beta_3$ binders (*i.e.* N-TIMP2$_{WT, RGD}$, Ala–N-TIMP2$_{WT, RGD}$, and N-TIMP2$_{HD}$) indicates that integrin $\alpha_v\beta_3$ is a more important contributor than MMP-14 to tube formation. Furthermore, the agonistic effect of FL-TIMP2 may be due to pro-MMP-2 activation in TIME cells by FL-TIMP2 at a concentration of 2 μM, an effect previously shown by others (25, 56).

In angiogenesis, the invasion of endothelial cells is a crucial step that is mediated by both MMP-14 and integrin $\alpha_v\beta_3$. Thus, the ability of the N-TIMP2 variants to inhibit this process was evaluated in a Boyden chamber Matrigel® invasion assay (Fig. 7). Treatment with cRGD (Fig. 7*I*) significantly inhibited invasiveness in TIME cells, with 21% inhibition (Fig. 7*J*). Although none of the mono-specific variants significantly inhibited the invasion process, all the bi-specific variants, N-TIMP2$_{WT, RGD}$ (Fig. 7*E*), N-TIMP2$_{5M, RGD}$ (Fig. 7*E*) and N-TIMP2$_{HD}$ (Fig. 7*I*), significantly inhibited this process, with 18, 14, and 28% of inhibition, respectively (Fig. 7*J*). Notably, in the invasion assay N-TIMP2$_{HD}$ proved to be a superior inhibitor to the bi-specific monomers (*i.e.* N-TIMP2$_{WT, RGD}$ and N-TIMP2$_{5M, RGD}$, $p < 0.05$) and to all the mono-specific proteins (*i.e.* N-TIMP2$_{WT}$, N-TIMP2$_{5M}$, and Ala–N-TIMP2$_{WT, RGD}$, $p < 0.05$).

N-TIMP2$_{HD}$ inhibits U87MG xenograft tumor growth in mice

Nude mice bearing subcutaneous U87MG xenografts were injected intra-tumor with N-TIMP2$_{HD}$. The untreated control group was injected intra-tumor with PBS. The growth rate of the tumors was slower in the N-TIMP2$_{HD}$–treated group, thereby demonstrating the anti-tumor activity of the bi-specific protein in an *in vivo* model (Fig. 8).

Discussion

A potential risk in the therapeutic targeting of MMPs (and other enzymatic multifamilies) is that these proteins do not work in isolation but as part of complex enzymatic cascades, in which each MMP may cross-activate other MMPs and/or other

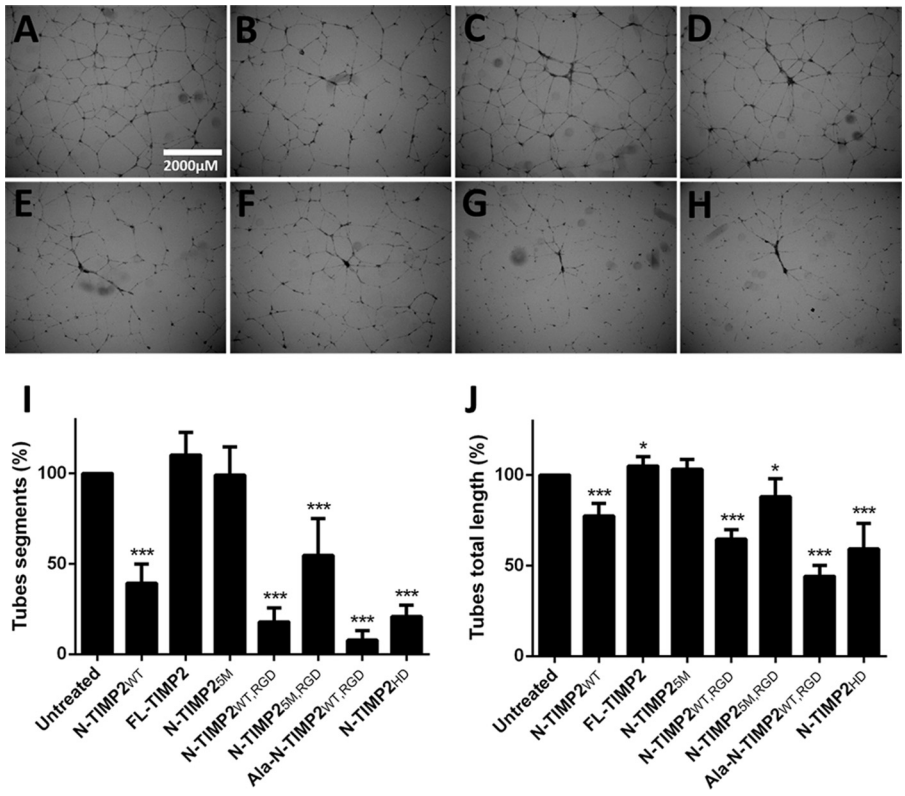

Figure 6. Inhibition of tube formation by N-TIMP2 variants. *A*, untreated cells. *B*, N-TIMP2$_{WT}$. *C*, FL-TIMP2. *D*, N-TIMP2$_{5M}$. *E*, N-TIMP2$_{WT, RGD}$. *F*, N-TIMP2$_{5M, RGD}$. *G*, Ala–N-TIMP2$_{WT, RGD}$. *H*, N-TIMP2$_{HD}$. *I*, quantification of the number of tube segments normalized to untreated cells. *J*, quantification of tube total length normalized to untreated cells. *Error bars* represent S.D. Statistical analysis was performed by Student's *t* test compared with the untreated control; *, $p < 0.05$; ***, $p < 0.0001$, $n = 6$.

proteins, which may compensate for their loss of function (61). An excellent example of such cross-reactivity is that of MMP-2 activation by MMP-14 (7, 21), a function that is facilitated by interaction of the former with integrin $\alpha_v\beta_3$ (21, 62, 63). Putative pathobiological roles have been ascribed to the MMP-14/MMP-2/integrin $\alpha_v\beta_3$ axis for a diverse array of cancers (20–22, 62), and this axis thus represents an attractive target for the development of novel cancer therapeutics.

We therefore evaluated the therapeutic potential of targeting this axis with novel bi-specific inhibitors acting against MMP-14 and integrin $\alpha_v\beta_3$. In parallel, studying these bi-specific inhibitors and their mono-specific counterparts allowed us to establish the roles of each target protein in important cancer pathways, such as MMP-2 activation, cancer, and endothelial cell invasion and tube formation.

From a practical point of view, the strength of dual-specificity targeting in anti-cancer therapeutics lies in its potential to abrogate the unwanted side effects of potent single-targeted MMP-14 or integrin $\alpha_v\beta_3$ inhibitors; such side effects are due to the roles that different MMPs and integrins play in homeostasis and other important normal biological functions, such as wound healing, cell adhesion, and cell differentiation (40, 64). It is likely that a dual-specific molecule would increase selectivity toward MMP-14 in preference to other MMPs via increased effective local concentrations due to the association of MMP-14 with integrin $\alpha_v\beta_3$. Moreover, a bi-specific inhibitor exhibiting synergistic effects only in cancerous tissues in which both MMP-14 and integrin $\alpha_v\beta_3$ are overexpressed and cross-react would contribute to target cell specificity. This notion is supported by the findings of Deryugina *et al.* (21) that MMP-14 and integrin $\alpha_v\beta_3$ are localized in close proximity on the cell surface, and their cross-reactivity and synergistic function strongly promote cancer cell invasion and maturation of pro-MMP-2 to active forms.

In keeping with the findings of Deryugina *et al.* (21), we showed by SPR that the bi-specific N-TIMP2 variants could simultaneously bind to MMP-14 and integrin $\alpha_v\beta_3$. We also showed that our wide range N-TIMP2 variants have different affinities and activities toward the two receptors (Table 1 and Fig. 2). A comparison of the inhibition of the two receptors separately and simultaneously aided us in defining the importance of the cross-talk between MMP-14 and integrin $\alpha_v\beta_3$ and in determining which of the two effectors plays the dominant role in a particular malignant process, namely MMP-2 activation, endothelial tube formation, and cancer cell invasion.

The superior inhibition of cancer and endothelial cell invasion by the heterodimeric variant N-TIMP2$_{HD}$ (*versus* the mono-specific and other bi-specific monomers) may be attributed to its ability to bind both receptors with the highest affinity relative to the other engineered proteins. In N-TIMP2$_{HD}$ (unlike in the other bi-specific N-TIMP2 monomers), the MMP-14 and integrin $\alpha_v\beta_3$ epitopes are relatively distant from one another, an arrangement that we believe allows optimal interaction with their respective targets. Indeed, the monomeric N-TIMP2$_{WT, RGD}$, which was less potent than

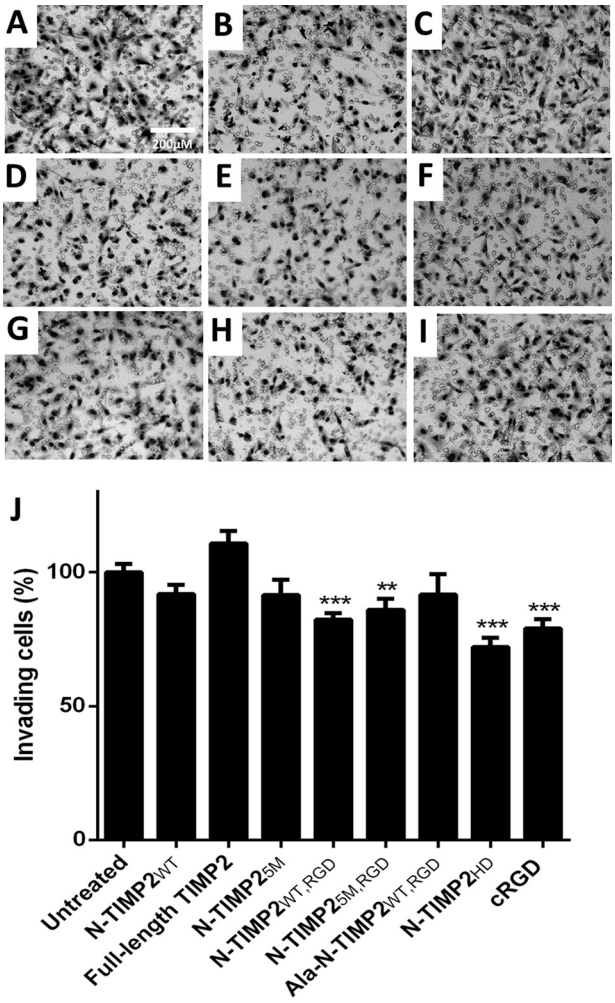

Figure 7. Inhibition of invasion of TIME cells by N-TIMP2 variants. *A,* untreated cells. *B,* N-TIMP2$_{WT}$. *C,* FL-TIMP2. *D,* N-TIMP2$_{5M}$. *E,* N-TIMP2$_{WT, RGD}$. *F,* N-TIMP2$_{5M, RGD}$. *G,* Ala–N-TIMP2$_{WT, RGD}$. *H,* N-TIMP2$_{HD}$. *I,* cRGD. *J,* quantification of invasive cells normalized to untreated cells. *Error bars* represent S.D. One-way ANOVA with Dunnett's multiple comparison with the untreated control was utilized for statistical analysis; **, $p < 0.005$; ***, $p < 0.001$, $n = 3$. A comparison between treatment with N-TIMP2$_{HD}$ *versus* all other treatments showed the statistically significant superior inhibition of N-TIMP2$_{HD}$ *versus* N-TIMP2$_{WT, RGD}$, N-TIMP2$_{5M, RGD}$, and Ala–N-TIMP2$_{WT, RGD}$ ($p < 0.05$); N-TIMP2$_{WT}$ and N-TIMP2$_{5M}$ ($p < 0.005$); and FL-TIMP2 ($p < 0.001$).

N-TIMP2$_{HD}$ in inhibiting cell invasion, showed decreased ability to simultaneously engage MMP-14 and integrin $\alpha_v\beta_3$ compared with N-TIMP2$_{HD}$ (Fig. 2, *E* and *F*). In addition, the bi-specific N-TIMP2$_{HD}$ was better than its mono-specific counterpart N-TIMP2$_{5M}$ (solely a MMP-14 binder) in its ability to inhibit cellular MMP-2 activation and cell invasion (Figs. 3, 5, and 7), despite having MMP-14 binding and inhibition potencies similar to those of N-TIMP2$_{5M}$ (Table 1). This finding is in agreement with the major role of integrin $\alpha_v\beta_3$ in MMP-2 activation, cell-surface localization, and cell invasion. The finding that N-TIMP2$_{HD}$ was also a better inhibitor than Ala–N-TIMP2$_{WT, RGD}$ (a strong integrin binder having reduced MMP-14 inhibition activity) illustrates the distinct contribution of MMP-14 to inhibiting MMP-2 activation and cell invasion. N-TIMP2$_{HD}$ was also superior to N-TIMP2$_{5M}$ and comparable with Ala–N-TIMP2$_{WT, RGD}$ in its ability to inhibit tube formation; this finding indicates a more dominant role for integrin $\alpha_v\beta_3$ than MMP-14 in capillary tube formation. However, as described previously by Stratman *et al.* (65), in cellular three-dimensional and *in vivo* angiogenesis models, MMP-14 may also play a significant role in angiogenesis. Thus, it is possible that our engineered bi-specific variants could exhibit a superior effect to the mono-specific integrin $\alpha_v\beta_3$ binder in the inhibition of angiogenesis *in vivo*.

Compared with the bi-specific monomeric N-TIMP2$_{5M, RGD}$, Ala–N-TIMP2$_{WT, RGD}$ exhibited inferior ability to inhibit MMP-2 activation, and N-TIMP2$_{5M}$ exhibited reduced ability to inhibit the intermediate MMP-2 processing to the matured form (Fig. 3), despite their higher binding to integrin $\alpha_v\beta_3$ and MMP-14, respectively. This finding again highlights the utility of integrin $\alpha_v\beta_3$ and MMP-14 dual targeting for superior inhibition of MMP-2 activation/processing. Notably, N-TIMP2$_{HD}$ exhibited better inhibition activity than N-TIMP2$_{5M, RGD}$ in both MMP-2 activation/processing and biological assays, which supports our premise that distancing the mutated counterparts would result in better biochemical and biological inhibitory effects.

In contrast to N-TIMP2$_{HD}$, FL-TIMP2 exhibited agonistic activity in the endothelial tube formation assay (Fig. 6), which is probably due to the interaction of its C-terminal domain with the hemopexin of pro-MMP-2, thereby bringing pro-MMP-2 to the cell surface where it is activated by MMP-14 (26). At low concentrations, FL-TIMP2 serves as an MMP-2 activator, although at high concentrations it acts as an inhibitor due to its interaction with and inhibition of most MMP-14 receptors (Fig. S6) (25, 27, 56). Notably, the C-terminal domain is absent in the engineered N-TIMP2 variants, which does not allow them to activate MMP-2 and to act as agonists (66).

The difference between the zymography results (Fig. 3), in which FL-TIMP2 inhibited MMP-2 processing, and its agonistic activity in the tube formation assay may result from the different incubation times for these experiments (48 h for zymography and 18–20 h for the other assays). In the 48-h incubation, significant amounts of endogenous FL-TIMP2 could be produced, and the full-length protein could thus act as an inhibitor for MMP-14–induced MMP-2 activation (56, 67, 68). Shorter incubation times might result in lower FL-TIMP2 production, and the protein would thus act as an activator, as shown previously (56, 67, 68). Because FL-TIMP2 is endogenously expressed by cancer cells, our inhibitors can compete with it in binding to MMP-14, a process that would (i) inhibit pro-cancerous activity resulting from FL-TIMP2 activity at low concentrations, and (ii) occupy MMP-14 receptors, thereby lowering the concentrations at which FL-TIMP2 acts as an inhibitor. These actions, together with the direct inhibition of MMP-14 and integrin $\alpha_v\beta_3$, may provide additional benefits for our engineered variants in the inhibition of endothelial tube formation and cell invasion.

The influence of our N-TIMP2 variants on MMP-2 is perhaps best reflected in our findings that Ala–N-TIMP2$_{WT, RGD}$ inhibited MMP-2 localization on the cell surface (Fig. 4). It is well known that matured MMP-2 is localized on the cell surface via integrin $\alpha_v\beta_3$ binding and that this docking increases cell invasiveness and angiogenesis (19, 29, 69). For technical reasons, we were not able to show that N-TIMP2$_{WT, RGD}$ and

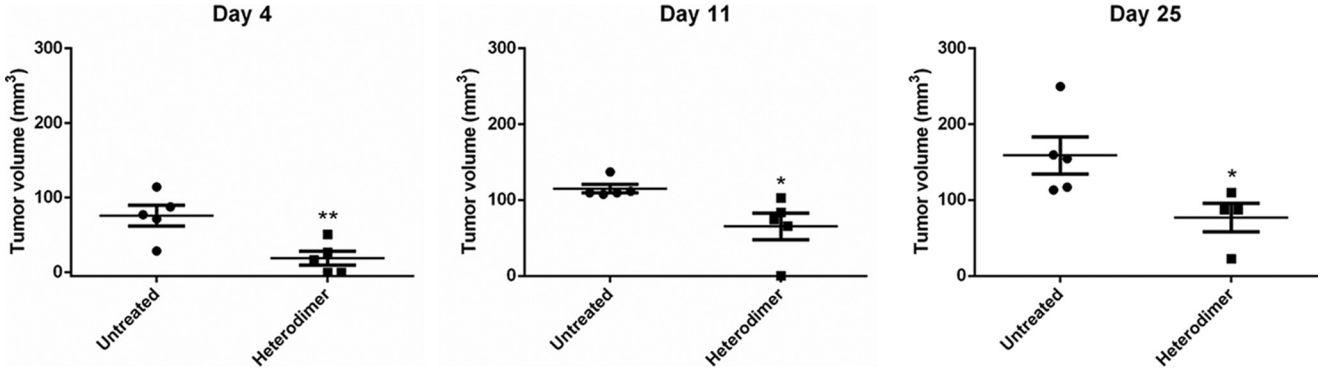

Figure 8. N-TIMP2$_{HD}$ inhibits U87MG xenograft growth in mice. Tumor size in mice treated with 500 nM N-TIMP2$_{HD}$ and in untreated (PBS) mice was monitored over 25 days. Measurements from days 4, 11, and 25 are shown. Each group contained five mice. At day 18, one mouse from the N-TIMP2$_{HD}$-treated group died during anesthesia. *Error bars* represent S.E. Statistical analysis was performed by Student's *t* test compared with the PBS-treated control; *, $p < 0.05$; **, $p < 0.001$.

N-TIMP2$_{HD}$ have the same MMP-2 removal activity as Ala–N-TIMP2$_{WT, RGD}$. Nonetheless, it seems reasonable to extrapolate the inhibition of MMP-2 localization on the cell surface by Ala–N-TIMP2$_{WT, RGD}$ to the bi-specific variants N-TIMP2$_{HD}$ and N-TIMP2$_{WT, RGD}$, because these two variants are similar to Ala–N-TIMP2$_{WT, RGD}$ in terms of integrin $\alpha_v\beta_3$ binding. We may therefore presume that N-TIMP2$_{HD}$ will strongly inhibit MMP-2 activation and prevent the docking of the matured MMP-2 on the cell surface.

In summary, our results suggest that MMP-14 inhibition is related to pro-MMP-2 processing, whereas inhibition of integrin $\alpha_v\beta_3$ contributes to the inhibition of intermediate MMP-2 activation (Fig. 3 and Table 2). Inhibition of integrin $\alpha_v\beta_3$ also plays a significant role in hindering tube formation, as reflected in the finding that Ala–N-TIMP2$_{WT, RGD}$, N-TIMP2$_{WT, RGD}$, and N-TIMP2$_{HD}$ were more active than N-TIMP2$_{5M, RGD}$ and N-TIMP2$_{WT}$ (Fig. 6 and Table 2). As we have shown here, tube formation is thus more closely influenced by integrin $\alpha_v\beta_3$ than by MMP-14 or MMP-2. In contrast, cell invasion is coupled to both integrin $\alpha_v\beta_3$ and MMP-14 activities, and simultaneous inhibition of the two receptors by N-TIMP2$_{HD}$ results in superior inhibition (Figs. 5*K* and 7*J* and Table 2). In more specific terms, in addition to generating new molecules that bind MMP-14 and integrin $\alpha_v\beta_3$, this study has generated, for the first time, single molecules that successfully interfere with all the components of the MMP-14/MMP-2/integrin $\alpha_v\beta_3$ axis and inhibit their biological activity. The study therefore indicates the utility of initiating pre-clinical studies of our engineered MMP-14- and integrin $\alpha_v\beta_3$-binding N-TIMP2 variant proteins.

Viewing the findings of this study within the broader context of the current drive to develop targeted cancer therapies reveals the implications of our approach for the future. In broad terms, our study illustrates a protein engineering strategy for producing bi-specific protein monomers and heterodimers as selective tumor-targeting agents with therapeutic potential. Even more importantly, we foresee that our strategy will generate a technology that can be broadly applied to targeting membrane receptors and soluble antigens in a variety of diseases.

Experimental procedures

MMP-14$_{CAT}$ protein production

The pET3a vector containing the human MMP-14 catalytic domain gene (MMP-14$_{CAT}$, residues 112–292) with a C-terminal His$_6$ tag (kindly provided by Irit Sagi, Weizmann Institute of Science, Israel) was expressed in *Escherichia coli* strain Bl21 (DE3) and purified as described previously (50). Following affinity chromatography using nickel-nitrilotriacetic acid-Sepharose beads (Invitrogen), CHAPS was added to a final concentration of 0.1% w/v, and the mixture was incubated for 3 days at 4 °C to digest the C-terminal hinge region of MMP-14 at residues 292–318. The protein was further purified on a gel-filtration Superdex 200 column (GE Healthcare) pre-equilibrated with buffer A (50 mM Tris, pH 7.5, 100 mM NaCl, 5 mM $CaCl_2$). The protein concentration was determined by UV-visible absorbance at 280 nm (extinction coefficient (ϵ_{280}) of 35,410 M^{-1} cm^{-1}) using a NanoDrop spectrophotometer (ThermoFisher Scientific). The purity of the protein was determined by SDS-PAGE and MS analysis (MALDI-TOF Reflex-IV, Ilse Katz Institute for Nanoscale Science and Technology, BGU, Israel). MMP-14$_{CAT}$ was labeled for 1 h at room temperature with DyLight-488 amine-reactive dye (ThermoFisher Scientific) in 0.05 M sodium borate buffer, pH 8.5, at a molar ratio of 1:5 (protein/dye). The labeled protein was washed free of unbound dye with buffer A in a Vivaspin (GE Healthcare) with a 5-kDa cutoff until no color was observed in the flow-through.

Construction and expression of yeast surface–displayed N-TIMP2$_{RGD}$ library

Yeast surface display is a powerful directed evolution technology in which proteins are displayed on the yeast surface through genetic fusion to the yeast mating agglutinin protein Aga2p (70). Aga2p is disulfide-bonded to Aga1p, which is covalently linked to the yeast cell wall. The protein of interest is flanked by epitope tags, which are used to confirm expression of the construct on the yeast cell surface and to quantify surface expression levels. Fluorescence-activated cell sorting (FACS)-based high-throughput screening of tens of millions of yeast-displayed mutated proteins allows for the rapid isolation of variants with altered properties, such as increased target affin-

Table 2
Summary of the variants' activities in different cellular assays
ND means inhibition was not detected.

Variant	Tube formation inhibition[a,b]	Invasion inhibition[b] of TIME cells	Invasion inhibition[b] of U87MG cells	Matured MMP-2 percentage[c]	Intermediate MMP-2 percentage	Total active MMP-2
	%	%	%	%	%	%
FL-TIMP2	−10[d]	−11[d]	−5[d]	3	0.6	3.6
N-TIMP2$_{WT}$	61	8	10	1.3	4.1	5.4
N-TIMP2$_{5M}$	1	8	8	2.5	0.5	3
N-TIMP2$_{WT, RGD}$	82	18	20	2.3	4.7	7
N-TIMP2$_{5M, RGD}$	45	14	−2.5	1.7	1.1	2.8
Ala- N-TIMP2$_{WT, RGD}$	92	8	13	2.4	4.9	7.3
N-TIMP2$_{HD}$	79	28	33	1.6	0.4	2
cRGD	ND	21	12	2.8	3.5	6.3

[a] Tube formation is measured as number of segments.
[b] Percent of inhibition was compared with the untreated control.
[c] For untreated cells, the percentages of the different MMP-2 forms are as follows: 3.9% for MMP-2 intermediate; 3.5% for MMP-2 matured; and 7.4% for total active MMP-2 (intermediate + matured).
[d] − represents activation.

ity. One of the benefits of yeast display over other protein engineering technologies, such as phage or mRNA display, is that multicolor FACS can be used to isolate clones with the desired target affinity by normalizing yeast expression levels with binding levels.

The pCTCON yeast surface display vector was digested and linearized with BamHI and Nhe-I. The N-TIMP2$_{WT}$ gene was amplified using PCR with homologous primers for pCTCON plasmids. PCR assembly with overlapping primers was used to prepare an N-TIMP2$_{RGD}$ library, in which positions 51–59 in N-TIMP2 were replaced with an RGD motif having three random amino acids flanking the motif on each side (underlined in the Ultra_RGD fragment, shown below). The assembly PCR products were amplified by PCR using homologous primers to the pCTCON construct: Fwd, 5′-GGTGGTTCTGGTGGTGGTGGTTCTGGTGGTGGTGGTTCTGCTAGCTGCAGCTGCTCCCCGGTG-3′, and Rev, 5′-GCTATTACAAGTCCTCTTCAGAAATAAGCTTTTGTTCAGATGGATCTTGGAAAGCCAATGGTTTATCTGGCAAGGATCCCTCGCAGCCCATCTGGTACC-3′.

The amplified gene along with the digested pCTCON linear vector were transformed by electroporation into *Saccharomyces cerevisiae* strain EBY100 by using recombinant homology as described previously (71). The library size was 1.75×10^7, as calculated by dilution plating on selective plates. The overlapping primers that were used for the assembly PCR were as follows: Ultra_1, 5′-TGCAGCTGCTCCCCGGTGCACCCGCAACAGGCGTTTTGCAATGCAGATGTAGTGATCAGGGCCAAAGCGGTCAGTGAGAAGGAAGTG-3′; Ultra_2, 5′-GCGGTCAGTGAGAAGGAAGTGGACTCTGGAAACGACATTTATGGCAACCCTATCAAGAGGATCCAGTATGAGATCAAGCAG-3′; Ultra_RGD, 5′-GAGGATCCAGTATGAGATCAAGCAGATANNSNNSNNSAGGGGGGACNNSNNSNNSATAGAGTTTATCTACACGGCCCCCTC-3′, where n = A, C, T, or G and S = C or G; Ultra_3, 5′-CCTTCTTTCCTCCAACGTCCAGCGAGACCCCACACACTGCCGAGGAGGGGGCCGTGTAGATAAACTC-3′; Ultra_4, 5′-CACGATGAAGTCACAGAGGGTGATGTGCATCTTGCCGTCCCCCTCGGCCTTTCCTGCAATGAGATATTCCTTCTTTCCTCCAACGTCCAG-3′; and Ultra_5, 5′-CTCGCAGCCCATCTGGTACCTGTGGTTCAGGCTCTTCTTCTGGGTGGTGCTCAGGGTGTCCCAGGGCACGATGAAGTCACAGAGGGTG-3′.

Screening of the N-TIMP2$_{RGD}$ library

The yeast-displayed N-TIMP2$_{RGD}$ library was grown in selective medium (yeast nitrogen base (6.7 g/liter), Na_2HPO_4 (5.4 g/liter), $NaH_2PO_4{\cdot}H_2O$ (8.56 g/liter), dextrose (20 g/liter), Bacto Casamino acids (5 g/liter)) and induced for expression with galactose (20 g/liter), as described previously (72). Yeast cells, $2–20 \times 10^6$, were sorted in each round against different concentrations of integrin $\alpha_v\beta_3$, as described previously with some modifications (4). Briefly, yeast cells were labeled with integrin $\alpha_v\beta_3$ (R&D Systems) and a 1:200 dilution of chicken anti-c-Myc antibody (Abcam) in integrin-binding buffer (IBB, 20 mM Tris, pH 7.5, 100 mM NaCl, 1 mM $MgCl_2$, 1 mM $MnCl_2$, 2 mM $CaCl_2$, and 1 mg/ml bovine serum albumin (BSA)) for 1 h at room temperature. Cells were washed and resuspended in ice-cold IBB containing a 1:25 dilution of FITC-labeled mouse anti-α_v integrin (BioLegend) and a 1:100 dilution of phycoerythrin (PE)-conjugated anti-chicken–IgY (Santa Cruz Biotechnology). After 30 min on ice, the cells were washed with IBB and sorted using a iCyt Synergy FACS apparatus (Sony Biotechnology). In the expression sort, only yeast cells expressing the intact N-TIMP2$_{RGD}$ proteins were selected (using the anti-c-Myc antibody). For the subsequent integrin $\alpha_v\beta_3$ affinity sorts, the concentrations of integrin $\alpha_v\beta_3$ that were added to the yeast cells decreased with each sort, as follows: 500 nM (sorts 1 and 2), 200 nM (sort 3), 50 nM (sort 4), and 20 nM (sort 5). In each integrin–$\alpha_v\beta_3$– binding sort, 0.3–2% of the yeast high-affinity (normalized to expression) cell population was collected using a diagonal sorting gate. After each sort round, the yeast plasmid DNA was purified using the Zymoprep™ yeast plasmid miniprep I kit (ZymoResearch). Thereafter, the plasmid was transformed into electrocompetent *E. coli* and grown overnight on ampicillin LB agar plates. Then, 20–40 colonies were transferred to ampicillin/LB culture medium and grown overnight at 37 °C. The plasmid was extracted from the bacteria using HiYield plasmid mini kit (RBC Bioscience) and was sequenced (Genetics Unit, National Institute of Biotechnology in the Negev, Ben-Gurion University of the Negev, Israel).

Construction of monomeric and dimeric N-TIMP2 variants

Using PCR, the alanine residue was added before Cys-1 of N-TIMP2$_{WT, RGD}$ so as to generate a mono-specific integrin $\alpha_v\beta_3$-only binding variant (Ala–N-TIMP2$_{WT, RGD}$). The following primers were applied: alanine pPic Fwd, 5′-GGTATCTCTCGAGAAAAGAGCATGCAGCTGCTCCCCG-3′, and pPic Rev, 5′-GCTGGCGGCCGCCTCGCAGCCCATCTGGTA-3′. N-TIMP2$_{5M, RGD}$ was generated by the insertion of the following five mutations into the N-TIMP2$_{WT, RGD}$ gene: M35I, D38N, N68S, G71V, and R97H (Integrated DNA Technologies). N-TIMP2$_{HD}$ comprising N-TIMP2$_{5M}$ linked to N-TIMP2$_{WT, RGD}$ with a flexible linker (SGGGGSGGGGSGGGGS) was generated by assembly PCR. First, the N-TIMP2$_{5M}$ gene was amplified with the primers: pPic Fwd, 5′-GGTATCTCTCGAGAAAAGATGCAGCTGCTCCCCG-3′, and linker Rev, 5′-AGAACCACCACCACCAGAACCACCACCACCAGAACCACCACCACCACTCTCGCAGCCCATCTGGTACC-3′, generating the product N-TIMP2$_{5M}$-linker gene. The N-TIMP2$_{WT, RGD}$ gene was amplified with the primers: Fwd linker, 5′-GGTGGTTCTGGTGGTGGTGGTTCTGGTGGTGGTGGTTCTTGCAGCTGCTCCCCGGTG-3′, and pPic Rev, generating the product linker-N-TIMP2$_{WT, RGD}$ gene. Then, assembly PCR was performed, using the linker–N-TIMP2$_{WT, RGD}$ gene as the template and the N-TIMP2$_{5M}$–linker gene and pPic Rev as primers.

Production and purification of soluble N-TIMP2 proteins

N-TIMP2-soluble protein was produced by utilizing methylotrophic *X33 Pichia pastoris* according to the pPICZα protocol (Invitrogen) and as described previously with modifications (38). Briefly, the different N-TIMP2 genes were cloned into pPICZαA vector for expression in the *X33 P. pastoris* strain. Proteins were prepared with both c-Myc and His$_6$ tags at the C terminus for protein detection and purification, respectively. N-TIMP2 proteins were purified from the yeast growth medium by affinity column chromatography using nickel-nitrilotriacetic acid–Sepharose beads (Invitrogen) equilibrated in a mixture of 50 mM Tris, pH 7.5, 300 mM NaCl, and 10 mM imidazole and eluted with a mixture of 50 mM Tris, pH 7.5, 300 mM NaCl, and 300 mM imidazole. Thereafter, separation on a gel-filtration Superdex 75 column (GE Healthcare), equilibrated in 50 mM Tris, pH 7.5, 300 mM NaCl, and 5 mM $CaCl_2$ at a flow rate of 0.5 ml/min on an ÄKTA pure instrument, was performed. Protein size was verified by SDS-PAGE and MS analysis (Ilse Katz Institute for Nanoscale Science and Technology, Ben-Gurion University of the Negev, Israel). Protein concentrations were determined by UV-visible absorbance at 280 nm, using a NanoDrop spectrophotometer (ϵ_{280} of 13,325 M^{-1} cm^{-1} for N-TIMP2$_{WT}$, N-TIMP2$_{WT, RGD}$, Ala–N-TIMP2$_{WT, RGD}$, and N-TIMP2$_{5M, RGD}$, and 26,650 M^{-1} cm^{-1} for N-TIMP2$_{HD}$). Purification yields for all proteins were 0.2–4 mg/liter.

Surface plasmon resonance experiments

The binding between MMP-14$_{CAT}$ and N-TIMP2 variants was detected using SPR spectroscopy on a ProteOn^{TM} XPR36 (Bio-Rad), as described previously (73) with modifications. Briefly, for MMP-14$_{CAT}$ binding, an HTG chip (Bio-Rad) was loaded with 150 μl of 10 mM $NiSO_4$ (pH 6.3) at a rate of 30 μl/min for 5 min. N-TIMP2 variants (0.0066 – 0.013 μg/μl, 150 μl) were then immobilized on the chip at a flow rate of 30 μl/min for 5 min; an empty channel was used as background. For determination of the affinity constants (K_D) of either N-TIMP2$_{5M, RGD}$ or N-TIMP2$_{HD}$ with MM-14$_{CAT}$, MMP-14$_{CAT}$ was diluted in a mixture of 50 mM Tris, pH 7.5, 100 mM NaCl, and 5 mM $CaCl_2$ to 3.1, 6.3, 12.5, 25, or 50 nM. For N-TIMP2$_{WT, RGD}$ and Ala–N-TIMP2$_{WT, RGD}$, the following concentrations of MM-14$_{CAT}$ were used: 31.3, 62.5, 125, 250, and 500 nM. The analyte, MMP-14$_{CAT}$, was allowed to flow over the chip at a flow rate of 25 μl/min for 981 s, followed by 20 min of dissociation. The response was monitored as a function of time at 25 °C, and the K_D values between the N-TIMP2 variants and MMP-14$_{CAT}$ were determined. For measuring the binding constants between N-TIMP2 variants and integrin $\alpha_v\beta_3$, a GLC chip (Bio-Rad) was loaded with 150 μl of the amine-coupling reagents, 0.1 M *N*-hydroxysuccinimide and 0.4 M 1-ethyl-3-(3-dimethylaminopropyl)-carbodiimide, at a rate of 30 μl/min for 5 min. Thereafter, 150 μl of 0.067 and 0.02 μg/μl of integrin $\alpha_v\beta_3$ and BSA, respectively, were immobilized to different channels at a flow rate of 30 μl/min for 5 min. The BSA channel was used as a control. N-TIMP2$_{WT, RGD}$ was diluted in IBB, without BSA, to 12.5, 25, 50, 100, or 200 nM and allowed to flow over the chip at a flow rate of 30 μl/min for 818 s. N-TIMP2$_{5M, RGD}$ was diluted to 9.4, 18.8, 37.5, 75, or 150 nM; Ala–N-TIMP2$_{WT, RGD}$ was diluted to 12.5, 25, 50, 100, or 200 nM, and N-TIMP2$_{HD}$ was diluted to 16.2, 32.4, 64.7, 129.4, or 258.8 nM. The three variants were allowed to flow over the chip at a rate of 40 μl/min for 613 s, followed by 20 min of dissociation. The K_D value between the N-TIMP2 variants and integrin $\alpha_v\beta_3$ was determined; the χ^2 values for all the analyses were less than 10%.

Dual receptor binding experiments with immobilized integrin $\alpha_v\beta_3$

Simultaneously, binding of N-TIMP2$_{WT, RGD}$ and N-TIMP2$_{HD}$ to both MMP-14 and integrin $\alpha_v\beta_3$ was tested using SPR. First, a GLC chip (Bio-Rad) was loaded with 0.02 μg/μl integrin $\alpha_v\beta_3$ and BSA as described previously. Then, IBB without BSA or 0.027 μg/μl of either N-TIMP2$_{WT, RGD}$ or N-TIMP2$_{HD}$ in IBB without BSA were allowed to flow over the chip at a flow rate of 30 μl/min for 300 s. Thereafter, 500 nM MMP-14 in IBB without BSA was allowed to flow over the chip at 30 μl/min for 437 s. The channel loaded with BSA served as a background control for integrin $\alpha_v\beta_3$ and MMP-14$_{CAT}$ binding. Injections of IBB without BSA buffer followed by MMP-14$_{CAT}$ in IBB without BSA served as a negative control. The dissociation of each complex in IBB without BSA was monitored for 600 s.

MMP-14$_{CAT}$ inhibition studies

The K_m value for the purified MMP-14$_{CAT}$ protein was determined by measuring MMP-14$_{CAT}$ activity against different concentrations (0–25 μM) of the fluorogenic substrate Mca-Pro-Leu-Gly-Leu-Dpa-Ala-Arg-NH_2·TFA (Merck Millipore) and fitting the data to the Michaelis-Menten equation (Equation 1) using Prism (GraphPad Software). The calculated value of K_m (16.79 ± 4.986 μM) and its standard error (S.E.) are

the average values that were obtained from three independent experiments.

The K_i determination was performed as described previously (38). The inhibition of the catalytic activity of MMP-14_{CAT} (0.005625 nM) against the fluorogenic substrate (7.5 μM) was tested using N-TIMP2_{WT} at 0.2–25 nM, N-TIMP$2_{WT, RGD}$ and Ala–N-TIMP$2_{WT, RGD}$ at 3.9–500 nM, and N-TIMP$2_{5M, RGD}$ and N-TIMP2_{HD} at 0.0075–0.125 nM. The K_i calculation was performed by utilizing Morrison's equation (Equation 2), the classic competitive inhibition equation for tight binding, by using Prism (GraphPad Software). K_i and its S.E. values were the average values obtained from three independent experiments,

$$V = \frac{V_{max}[S]}{K_m + [S]} \quad \text{(Eq. 1)}$$

where V is enzyme velocity; V_{max} is enzyme maximum velocity achieved at maximum substrate concentration; S is substrate concentration, and K_m is Michaelis-Menten constant,

$$\frac{V_i}{V_0} = 1 - \frac{([E] + [I] + K_i^{app}) - \sqrt{([E] + [I] + K_i^{app})^2 - 4[E][I]}}{2[E]} \quad \text{(Eq. 2)}$$

where V_i is enzyme velocity in the presence of inhibitor; V_0 is enzyme velocity in the absence of inhibitor; E is enzyme concentration; I is inhibitor concentration; S is substrate concentration; K_m is Michaelis-Menten constant, and K_i^{app} is the apparent inhibition constant, which is given by Equation 3,

$$K_i^{app} = K_i\left(1 + \frac{[S]}{K_m}\right) \quad \text{(Eq. 3)}$$

where K_i is the inhibition constant.

Cell cultures

TIME cells (ATCC) were maintained in vascular cell basal medium (ATCC) supplemented with 2% fetal bovine serum (FBS) and growth factor supplements (ATCC). The U87MG glioblastoma cell line (ATCC) was maintained in DMEM (Biological Industries) supplemented with 10% FBS (ThermoFisher Scientific), 1% L-glutamine (Biological Industries), and 1% penicillin/streptomycin (Biological Industries).

MMP-14 and integrin $\alpha_v\beta_3$ expression in U87MG and TIME cell lines

MMP-14 and integrin $\alpha_v\beta_3$ expression on U87MG and TIME cells was evaluated using an Accuri C6 flow cytometer (BD Biosciences). For MMP-14 detection, rabbit anti-MMP-14 antibody (Abgent) was applied, followed by goat anti-rabbit IgG-PE staining (Santa Cruz Biotechnology). Integrin $\alpha_v\beta_3$ was detected using anti-integrin $\alpha_v\beta_3$ antibody FITC-conjugated (LM609, Chemicon).

Inhibition of MMP-2 activation

A gelatin zymography assay was utilized to assess the ability of N-TIMP2 variants and FL-TIMP2 (R&D Systems) to inhibit cellular MMP-2 activation. U87MG cells (1.9×10^5) were grown on 96-well plates for 24 h. Then, cells were washed twice with serum-free DMEM and treated with 100 nM N-TIMP2 proteins in DMEM serum-free medium at 37 °C, 5% CO_2. In addition, different concentrations of FL-TIMP2 (1, 10, and 100 nM) and of cRGD (100 nM and 1 μM) were tested for their pro-MMP-2 activation activity. After 48 h, the medium was collected and centrifuged for 5 min at 10,000 × g. The medium was loaded on gelatin gel, washed for 1 h in 2.5% Triton X-100, and incubated overnight in a developer buffer (50 mM Tris, pH 7.4, 10 mM $CaCl_2$, and 0.02% NaN_3) at 37 °C, as described previously (74). Gels were stained with SimplyBlue™ SafeStain (ThermoFisher Scientific) and captured with MiniBIS Pro (DNR Bio-Imaging Systems). The intensity of the white bands was quantified using ImageJ.

Inhibition of MMP-2 cell surface localization

Flow cytometry analysis was used to detect recombinant matured MMP-2 on the U87MG cell surface. U87MG cells were grown to 70–80% confluence. Cells (10^5) were washed three times with IBB + 0.1% BSA, followed by 2 h of incubation with 100 nM recombinant matured MMP-2 (BioLegend) and 2 μM Ala–N-TIMP$2_{WT, RGD}$ at 4 °C. Cells were washed three times with IBB + 0.1% BSA and then incubated with mouse monoclonal anti-MMP2 antibody (clone CA-4001, Abcam) for 1 h at 4 °C. Cells were washed three times with IBB + 0.1% BSA and were labeled for 30 min at 4 °C with PE-conjugated goat anti-mouse IgG (1:50 dilution, Sigma). Cells were washed three times with IBB + 0.1% BSA, and MMP-2 levels on cell surface were detected with an Accuri C6 flow cytometer (BD Biosciences).

To determine which form of MMP-2 was removed from the U87MG cell surface by Ala–N-TIMP$2_{WT, RGD}$, a cell lysate was subjected to gelatin zymography, as described previously (21). Briefly, U87MG cells (2×10^5) were grown overnight on a 24-well plate. Then, the growth medium was replaced with a DMEM serum-free medium containing 2 μM Ala–N-TIMP$2_{WT, RGD}$. After a 48-h incubation, cells were washed three times with PBS. Thereafter, PBS (100 μl) was added to each well, and cells were scraped from the plate. Scraped cells from two wells were centrifuged, and the cell pellet was lysed with 35 μl of SDS sample buffer (4% SDS, 20% glycerol, 10% 2-mercaptoethanol, 0.004% bromphenol blue, and 0.125 M Tris HCl, pH 6.8) and incubated for 30 min at 37 °C. Thereafter, 50% glycerol (1:1 ratio) was added. The cell lysate (30 μl) was loaded on a gelatin gel, washed for 1 h in 2.5% Triton X-100, and incubated overnight in developer buffer at 37 °C.

To confirm that our inhibitor did indeed disrupt MMP-2 docking on integrin $\alpha_v\beta_3$, we utilized a solid-phase assay, as described previously (21). Wells of a 96-well ELISA plate were coated with 75 μl of integrin $\alpha_v\beta_3$ (2 μg/ml in PBS) and incubated overnight at 4 °C. The plate was washed three times with PBS, followed by blocking with 5% BSA. Then, 150 μl of U87MG serum-free medium obtained after 48 h of cell growth, which contained all the MMP-2 forms (pro/intermediate/matured), was added to each well, together with 2 μM of either Ala–N-TIMP$2_{WT, RGD}$ or cRGD, and the plate was incubated overnight at 4 °C. The plate was washed three times with PBS. Thereafter, the bound MMP-2 was solubilized with 25 μl of

SDS sample buffer, and the contents of the three wells were combined and loaded on gelatin zymography gels (30 μl). Gels were stained with SimplyBlue™ SafeStain and captured with MiniBIS Pro. The bound MMP-2 was detected by the appearance of white bands, the intensity of which was quantified using ImageJ. All the assays of the inhibition of MMP-2 cell surface localization were performed in triplicate.

Boyden chamber invasion assay

An *in vitro* Boyden chamber assay was performed using ThinCert™ 24-well inserts (Greiner Bio-One), as described previously with minor modifications (75). ThinCert™ cell culture insert membranes were coated with Matrigel® diluted (1:30) with either DMEM without serum or vascular cell basal medium in the upper compartment. The lower compartment of the chamber was filled with 600 μl of either DMEM or vascular cell basal medium supplemented with 2% serum for U87MG or TIME cells, respectively. U87MG (1.5×10^4) or TIME (2×10^4) cells were treated with 100 nM N-TIMP2 variants in 200 μl of serum-free DMEM or 2 μM N-TIMP2 variants in 200 μl of vascular cell basal medium, respectively. A mixture of 100 nM of each N-TIMP2$_{WT, RGD}$ and N-TIMP2$_{5M}$ was also used as a treatment for the U87MG cell line. The treatments were added to the pre-coated ThinCert™ cell culture inserts, which were then incubated for 20 h at 37 °C under 5% CO_2. Invasive cells were stained with Dipp Kwik Differential Stain Kit (American Mastertech Scientific) and were detected by EVOS FL Cell Imaging System (ThermoFisher Scientific) at ×20 magnification. The experiment was performed in triplicate; 15 fields were counted for each treatment, and the average of cells per field was determined.

Tube formation assay

A tube formation assay was utilized as described previously with minor modifications (76). Briefly, growth factor-reduced Matrigel® (GFR-Matrigel, Corning) was thawed overnight at 4 °C on ice. Thereafter, 150 μl of GFR-Matrigel were inserted into each well of 48-well plates, followed by centrifugation at $300 \times g$ for 15 min at 4 °C and incubation at 37 °C for 1 h. TIME cells (3.25×10^4) were then resuspended with 2 μM N-TIMP2 variants and FBS (2%) at a final volume of 200 μl, and the suspension was seeded on the Matrigel-coated plate. The plate was incubated at 37 °C under 5% CO_2 for 18 h and was monitored using EVOS FL Cell Imaging System at ×2 magnification. Six repetitions were performed, and the tube total lengths and the numbers of segments were analyzed and quantified using ImageJ Angiogenesis plug-in.

Xenograft model

U87MG cells (5×10^6) in 100 μl of serum-free DMEM, in the presence or absence of 500 nM N-TIMP2$_{HD}$, were mixed with 100 μl of Matrigel and injected subcutaneously into 6-week-old male Hsd/athymic nude–Foxn1nu mice (Envigo), as described previously (77, 78). Tumor growth was monitored over 25 days. Tumor size was measured with a caliper three times a week, and each measurement was followed by an additional intra-tumor injection of 50 μl of PBS containing 500 nM N-TIMP2$_{HD}$ to the treated group or 50 μl of PBS to the control group (a total of three injections per week for the entire experiment). Tumor volume was determined according to Equation 4,

$$V = \frac{L \times W^2}{2} \qquad \text{(Eq. 4)}$$

where L is length, and W is width.

All the animal experiments were conducted using protocols approved by the Committee of Use and Care of Animals at Ben-Gurion University of the Negev, and the animals were housed and handled according to the Unit for Laboratory Animal Medicine guidelines at Ben-Gurion University.

Author contributions—G. Y. and V. A. data curation; G. Y. and N. P. formal analysis; G. Y. and N. P. validation; G. Y. and N. P. investigation; G. Y. and V. A. methodology; G. Y. and N. P. writing-original draft; G. Y., V. A., and N. P. writing-review and editing; N. P. conceptualization; N. P. resources; N. P. supervision; N. P. funding acquisition; N. P. visualization.

Acknowledgments—We thank Dr. Alon Zilka, Lidan Aharon, and Yuval Zur for their technical assistance.

References

1. Hynes, R. O. (2002) Integrins: bidirectional, allosteric signaling machines. *Cell* **110,** 673–687 CrossRef Medline
2. Alghisi, G. C., and Rüegg, C. (2006) Vascular integrins in tumor angiogenesis: mediators and therapeutic targets. *Endothelium* **13,** 113–135 CrossRef Medline
3. Mizejewski, G. J. (1999) Role of integrins in cancer: survey of expression patterns. *Proc. Soc. Exp. Biol. Med.* **222,** 124–138 CrossRef Medline
4. Nomura, H., Sato, H., Seiki, M., Mai, M., and Okada, Y. (1995) Expression of membrane-type matrix metalloproteinase in human gastric carcinomas. *Cancer Res.* **55,** 3263–3266 Medline
5. Zhang, W., Matrisian, L. M., Holmbeck, K., Vick, C. C., and Rosenthal, E. L. (2006) Fibroblast-derived MT1-MMP promotes tumor progression *in vitro* and *in vivo*. *BMC Cancer* **6,** 52 CrossRef Medline
6. Li, X.-Y., Ota, I., Yana, I., Sabeh, F., and Weiss, S. J. (2008) Molecular dissection of the structural machinery underlying the tissue-invasive activity of membrane type-1 matrix metalloproteinase. *Mol. Biol. Cell* **19,** 3221–3233 CrossRef Medline
7. Stetler-Stevenson, W. G. (1999) Matrix metalloproteinases in angiogenesis: a moving target for therapeutic intervention. *J. Clin. Invest.* **103,** 1237–1241 CrossRef Medline
8. Sato, H., and Takino, T. (2010) Coordinate action of membrane-type matrix metalloproteinase-1 (MT1-MMP) and MMP-2 enhances pericellular proteolysis and invasion. *Cancer Sci.* **101,** 843–847 CrossRef Medline
9. Kikuchi, R., Noguchi, T., Takeno, S., Kubo, N., and Uchida, Y. (2000) Immunohistochemical detection of membrane-type-1-matrix metalloproteinase in colorectal carcinoma. *Br. J. Cancer* **83,** 215–218 CrossRef Medline
10. Hofmann, U. B., Westphal, J. R., Zendman, A. J., Becker, J. C., Ruiter, D. J., and van Muijen, G. N. (2000) Expression and activation of matrix metalloproteinase-2 (MMP-2) and its co-localization with membrane-type 1 matrix metalloproteinase (MT1-MMP) correlate with melanoma progression. *J. Pathol.* **191,** 245–256 CrossRef Medline
11. Nakamura, H., Ueno, H., Yamashita, K., Shimada, T., Yamamoto, E., Noguchi, M., Fujimoto, N., Sato, H., Seiki, M., and Okada, Y. (1999) Enhanced production and activation of progelatinase A mediated by membrane-type I matrix metalloproteinase in human papillary thyroid carcinomas. *Cancer Res.* **59,** 467–473 Medline
12. Kumar, C. C., Malkowski, M., Yin, Z., Tanghetti, E., Yaremko, B., Nechuta, T., Varner, J., Liu, M., Smith, E. M., Neustadt, B., Presta, M., and Armstrong, L. (2001) Inhibition of angiogenesis and tumor growth by

SCH221153, a dual α(v)β3 and α(v)β5 integrin receptor antagonist. *Cancer Res.* **61,** 2232–2238 Medline
13. Albelda, S. M., Mette, S. A., Elder, D. E., Stewart, R., Damjanovich, L., Herlyn, M., and Buck, C. A. (1990) Integrin distribution in malignant melanoma: association of the β3 subunit with tumor progression. *Cancer Res.* **50,** 6757–6764 Medline
14. Weis, S. M., and Cheresh, D. A. (2011) Tumor angiogenesis: molecular pathways and therapeutic targets. *Nat. Med.* **17,** 1359–1370 CrossRef Medline
15. Genís, L., Gálvez, B. G., Gonzalo, P., and Arroyo, A. G. (2006) MT1-MMP: universal or particular player in angiogenesis? *Cancer Metastasis Rev.* **25,** 77–86 CrossRef Medline
16. Deryugina, E. I., Ratnikov, B. I., Yu, Q., Baciu, P. C., Rozanov, D. V., and Strongin, A. Y. (2004) Prointegrin maturation follows rapid trafficking and processing of MT1-MMP in Furin-negative colon carcinoma LoVo cells. *Traffic* **5,** 627–641 CrossRef Medline
17. Stefanidakis, M., and Koivunen, E. (2006) Cell-surface association between matrix metalloproteinases and integrins: role of the complexes in leukocyte migration and cancer progression. *Blood* **108,** 1441–1450 CrossRef Medline
18. Gálvez, B. G., Matías-Román, S., Yáñez-Mó, M., Sánchez-Madrid, F., and Arroyo, A. G. (2002) ECM regulates MT1-MMP localization with β1 or αvβ3 integrins at distinct cell compartments modulating its internalization and activity on human endothelial cells. *J. Cell Biol.* **159,** 509–521 CrossRef Medline
19. Brooks, P. C., Strömblad, S., Sanders, L. C., von Schalscha, T. L., Aimes, R. T., Stetler-Stevenson, W. G., Quigley, J. P., and Cheresh, D. A. (1996) Localization of matrix metalloproteinase MMP-2 to the surface of invasive cells by interaction with integrin αvβ3. *Cell* **85,** 683–693 CrossRef Medline
20. Deshane, J., Garner, C. C., and Sontheimer, H. (2003) Chlorotoxin inhibits glioma cell invasion via matrix metalloproteinase-2. *J. Biol. Chem.* **278,** 4135–4144 CrossRef Medline
21. Deryugina, E. I., Ratnikov, B., Monosov, E., Postnova, T. I., DiScipio, R., Smith, J. W., and Strongin, A. Y. (2001) MT1-MMP initiates activation of pro-MMP-2 and integrin αvβ3 promotes maturation of MMP-2 in breast carcinoma cells. *Exp. Cell Res.* **263,** 209–223 CrossRef Medline
22. Hofmann, U. B., Westphal, J. R., Van Kraats, A. A., Ruiter, D. J., and Van Muijen, G. N. (2000) Expression of integrin α(v)β(3) correlates with activation of membrane-type matrix metalloproteinase-1 (MT1-MMP) and matrix metalloproteinase-2 (MMP-2) in human melanoma cells *in vitro* and *in vivo*. *Int. J. Cancer* **87,** 12–19 CrossRef Medline
23. Deryugina, E. I., Bourdon, M. A., Jungwirth, K., Smith, J. W., and Strongin, A. Y. (2000) Functional activation of integrin αvβ3 in tumor cells expressing membrane-type 1 matrix metalloproteinase. *Int. J. Cancer* **86,** 15–23 CrossRef Medline
24. Deryugina, E. I., Ratnikov, B. I., Postnova, T. I., Rozanov, D. V., and Strongin, A. Y. (2002) Processing of integrin αv subunit by membrane type 1 matrix metalloproteinase stimulates migration of breast carcinoma cells on vitronectin and enhances tyrosine phosphorylation of focal adhesion kinase. *J. Biol. Chem.* **277,** 9749–9756 CrossRef Medline
25. Butler, G. S., Butler, M. J., Atkinson, S. J., Will, H., Tamura, T., Schade van Westrum, S., Crabbe, T., Clements, J., d'Ortho, M. P., and Murphy, G. (1998) The TIMP2 membrane type 1 metalloproteinase "receptor" regulates the concentration and efficient activation of progelatinase A. A kinetic study. *J. Biol. Chem.* **273,** 871–880 CrossRef Medline
26. Itoh, Y., and Seiki, M. (2004) MT1-MMP: an enzyme with multidimensional regulation. *Trends Biochem. Sci.* **29,** 285–289 CrossRef Medline
27. Hernandez-Barrantes, S., Toth, M., Bernardo, M. M., Yurkova, M., Gervasi, D. C., Raz, Y., Sang, Q. A., and Fridman, R. (2000) Binding of active (57 kDa) membrane type 1-matrix metalloproteinase (MT1-MMP) to tissue inhibitor of metalloproteinase (TIMP)-2 regulates MT1-MMP processing and pro-MMP-2 activation. *J. Biol. Chem.* **275,** 12080–12089 CrossRef Medline
28. Pei, D., and Weiss, S. J. (1996) Transmembrane-deletion mutants of the membrane-type matrix metalloproteinase-1 process progelatinase A and express intrinsic matrix-degrading activity. *J. Biol. Chem.* **271,** 9135–9140 CrossRef Medline
29. Silletti, S., Kessler, T., Goldberg, J., Boger, D. L., and Cheresh, D. A. (2001) Disruption of matrix metalloproteinase 2 binding to integrin αvβ3 by an organic molecule inhibits angiogenesis and tumor growth *in vivo*. *Proc. Natl. Acad. Sci. U.S.A.* **98,** 119–124 CrossRef Medline
30. Kummar, S., Chen, H. X., Wright, J., Holbeck, S., Millin, M. D., Tomaszewski, J., Zweibel, J., Collins, J., and Doroshow, J. H. (2010) Utilizing targeted cancer therapeutic agents in combination: novel approaches and urgent requirements. *Nat. Rev. Drug Discov.* **9,** 843–856 CrossRef Medline
31. Gridelli, C., Rossi, A., Ciardiello, F., De Marinis, F., Crinò, L., Morabito, A., Morgillo, F., Montanino, A., Daniele, G., Piccirillo, M. C., Normanno, N., Gallo, C., and Perrone, F. (2016) BEVERLY: rationale and design of a randomized open-label phase III trial comparing Bevacizumab plus Erlotinib versus Erlotinib alone as first-line treatment of patients with EGFR-mutated advanced nonsquamous non-small-cell lung cancer. *Clin. Lung Cancer* **17,** 461–465 CrossRef Medline
32. Al-Lazikani, B., Banerji, U., and Workman, P. (2012) Combinatorial drug therapy for cancer in the post-genomic era. *Nat. Biotechnol.* **30,** 679–692 CrossRef Medline
33. Miles, D., von Minckwitz, G., and Seidman, A. D. (2002) Combination versus sequential single-agent therapy in metastatic breast cancer. *Oncologist* **7,** Suppl. 6, 13–19 Medline
34. Yap, T. A., Omlin, A., and de Bono, J. S. (2013) Development of therapeutic combinations targeting major cancer signaling pathways. *J. Clin. Oncol.* **31,** 1592–1605 CrossRef Medline
35. Papo, N., Silverman, A. P., Lahti, J. L., and Cochran, J. R. (2011) Antagonistic VEGF variants engineered to simultaneously bind to and inhibit VEGFR2 and αvβ3 integrin. *Proc. Natl. Acad. Sci. U.S.A.* **108,** 14067–14072 CrossRef Medline
36. May, C., Sapra, P., and Gerber, H. P. (2012) Advances in bispecific biotherapeutics for the treatment of cancer. *Biochem. Pharmacol.* **84,** 1105–1112 CrossRef Medline
37. McDonagh, C. F., Huhalov, A., Harms, B. D., Adams, S., Paragas, V., Oyama, S., Zhang, B., Luus, L., Overland, R., Nguyen, S., Gu, J., Kohli, N., Wallace, M., Feldhaus, M. J., Kudla, A. J., *et al.* (2012) Antitumor activity of a novel bispecific antibody that targets the ErbB2/ErbB3 oncogenic unit and inhibits heregulin-induced activation of ErbB3. *Mol. Cancer Ther.* **11,** 582–593 CrossRef Medline
38. Arkadash, V., Yosef, G., Shirian, J., Cohen, I., Horev, Y., Grossman, M., Sagi, I., Radisky, E. S., Shifman, J. M., and Papo, N. (2017) Development of high affinity and high specificity inhibitors of matrix metalloproteinase 14 through computational design and directed evolution. *J. Biol. Chem.* **292,** 3481–3495 CrossRef Medline
39. Folgueras, A. R., Pendás, A. M., Sánchez, L. M., and López-Otin, C. (2004) Matrix metalloproteinases in cancer: from new functions to improved inhibition strategies. *Int. J. Dev. Biol.* **48,** 411–424 CrossRef Medline
40. Decock, J., Thirkettle, S., Wagstaff, L., and Edwards, D. R. (2011) Matrix metalloproteinases: protective roles in cancer. *J. Cell. Mol. Med.* **15,** 1254–1265 CrossRef Medline
41. López-Otín, C., Palavalli, L. H., and Samuels, Y. (2009) Protective roles of matrix metalloproteinases: from mouse models to human cancer. *Cell Cycle* **8,** 3657–3662 CrossRef Medline
42. Nuti, E., Tuccinardi, T., and Rossello, A. (2007) Matrix metalloproteinase inhibitors: new challenges in the era of post broad-spectrum inhibitors. *Curr. Pharm. Des.* **13,** 2087–2100 CrossRef Medline
43. Hidalgo, M., and Eckhardt, S. G. (2001) Development of matrix metalloproteinase inhibitors in cancer therapy. *J. Natl. Cancer Inst.* **93,** 178–193 CrossRef Medline
44. Devy, L., Huang, L., Naa, L., Yanamandra, N., Pieters, H., Frans, N., Chang, E., Tao, Q., Vanhove, M., Lejeune, A., van Gool, R., Sexton, D. J., Kuang, G., Rank, D., Hogan, S., *et al.* (2009) Selective inhibition of matrix metalloproteinase-14 blocks tumor growth, invasion, and angiogenesis. *Cancer Res.* **69,** 1517–1526 CrossRef Medline
45. Plow, E. F., Haas, T. A., Zhang, L., Loftus, J., and Smith, J. W. (2000) Ligand binding to integrins. *J. Biol. Chem.* **275,** 21785–21788 CrossRef Medline
46. Li, R., Hoess, R. H., Bennett, J. S., and DeGrado, W. F. (2003) Use of phage display to probe the evolution of binding specificity and affinity in integrins. *Protein Eng.* **16,** 65–72 CrossRef Medline

47. Brew, K., and Nagase, H. (2010) The tissue inhibitors of metalloproteinases (TIMPs): an ancient family with structural and functional diversity. *Biochim. Biophys. Acta* **1803,** 55–71 CrossRef Medline
48. Sharabi, O., Shirian, J., Grossman, M., Lebendiker, M., Sagi, I., and Shifman, J. (2014) Affinity- and specificity-enhancing mutations are frequent in multispecific interactions between TIMP2 and MMPs. *PLoS ONE* **9,** e93712 CrossRef Medline
49. Bahudhanapati, H., Zhang, Y., Sidhu, S. S., and Brew, K. (2011) Phage display of tissue inhibitor of metalloproteinases-2. *J. Biol. Chem.* **286,** 31761–31770 CrossRef Medline
50. Ogata, H., Decaneto, E., Grossman, M., Havenith, M., Sagi, I., Lubitz, W., and Knipp, M. (2014) Crystallization and preliminary X-ray crystallographic analysis of the catalytic domain of membrane type 1 matrix metalloproteinase. *Acta Crystallogr. F Struct. Biol. Commun.* **70,** 232–235 CrossRef Medline
51. Wingfield, P., Sax, J. K., Stahl, S. J., Kaufman, J., Palmer, I., Chung, V., Corcoran, M. L., Kleiner, D. E., and Stetler-Stevenson, W. G. (1999) Biophysical and functional characterization of full-length, recombinant human tissue inhibitor of metalloproteinases-2 (TIMP-2) produced in *Escherichia coli*. *J. Biol. Chem.* **274,** 21362–21368 CrossRef Medline
52. Azzam, H. S., Arand, G., Lippman, M. E., and Thompson, E. W. (1993) Association of MMP-2 activation potential with metastatic progression in human breast cancer cell lines independent of MMP-2 production. *J. Natl. Cancer Inst.* **85,** 1758–1764 CrossRef Medline
53. Toth, M., and Fridman, R. (2001) Assessment of gelatinases (MMP-2 and MMP-9) by gelatin zymography. *Methods Mol. Med.* **57,** 163–174 Medline
54. Werb, Z. (1997) ECM and cell surface proteolysis: regulating cellular ecology. *Cell* **91,** 439–442 CrossRef Medline
55. Lafleur, M. A., Hollenberg, M. D., Atkinson, S. J., Knäuper, V., Murphy, G., and Edwards, D. R. (2001) Activation of pro-(matrix metalloproteinase-2) (pro-MMP-2) by thrombin is membrane-type-MMP-dependent in human umbilical vein endothelial cells and generates a distinct 63 kDa active species. *Biochem. J.* **357,** 107–115 CrossRef Medline
56. Lu, K. V., Jong, K. A., Rajasekaran, A. K., Cloughesy, T. F., and Mischel, P. S. (2004) Upregulation of tissue inhibitor of metalloproteinases (TIMP)-2 promotes matrix metalloproteinase (MMP)-2 activation and cell invasion in a human glioblastoma cell line. *Lab. Invest.* **84,** 8–20 CrossRef Medline
57. Dechantsreiter, M. A., Planker, E., Mathä, B., Lohof, E., Hölzemann, G., Jonczyk, A., Goodman, S. L., and Kessler, H. (1999) *N*-Methylated cyclic RGD peptides as highly active and selective $\alpha(v)\beta(3)$ integrin antagonists. *J. Med. Chem.* **42,** 3033–3040 CrossRef Medline
58. Johanns, M., Lemoine, P., Janssens, V., Grieco, G., Moestrup, S. K., Nielsen, R., Christensen, E. I., Courtoy, P. J., Emonard, H., Marbaix, E., and Henriet, P. (2017) Cellular uptake of proMMP-2:TIMP-2 complexes by the endocytic receptor megalin/LRP-2. *Sci. Rep.* **7,** 4328 CrossRef Medline
59. Folkman, J., and Haudenschild, C. (1980) Angiogenesis *in vitro*. *Nature* **288,** 551–556 CrossRef Medline
60. Seo, D. W., Li, H., Guedez, L., Wingfield, P. T., Diaz, T., Salloum, R., Wei, B. Y., and Stetler-Stevenson, W. G. (2003) TIMP-2 mediated inhibition of angiogenesis: an MMP-independent mechanism. *Cell* **114,** 171–180 CrossRef Medline
61. Ducharme, A., Frantz, S., Aikawa, M., Rabkin, E., Lindsey, M., Rohde, L. E., Schoen, F. J., Kelly, R. A., Werb, Z., Libby, P., and Lee, R. T. (2000) Targeted deletion of matrix metalloproteinase-9 attenuates left ventricular enlargement and collagen accumulation after experimental myocardial infarction. *J. Clin. Invest.* **106,** 55–62 CrossRef Medline
62. Baciu, P. C., Suleiman, E. A., Deryugina, E. I., and Strongin, A. Y. (2003) Membrane type-1 matrix metalloproteinase (MT1-MMP) processing of pro-αv integrin regulates cross-talk between $\alpha v\beta 3$ and $\alpha 2\beta 1$ integrins in breast carcinoma cells. *Exp. Cell Res.* **291,** 167–175 CrossRef Medline
63. Gonzalo, P., Moreno, V., and Ga, B. G. (2010) MT1-MMP and integrins: hand-to-hand in cell communication. *Biofactors* **36,** 248–254 CrossRef
64. Srichai, M. B., and Zent, R. (2010) in *Integrin Structure and Function* (Zent, R., and Srichai, M. B., eds), Springer, New York
65. Stratman, A. N., Saunders, W. B., Sacharidou, A., Koh, W., Fisher, K. E., Zawieja, D. C., Davis, M. J., and Davis, G. E. (2009) Endothelial cell lumen and vascular guidance tunnel formation requires MT1-MMP-dependent proteolysis in 3-dimensional collagen matrices. *Blood* **114,** 237–247 CrossRef Medline
66. Morgunova, E., Tuuttila, A., Bergmann, U., and Tryggvason, K. (2002) Structural insight into the complex formation of latent matrix metalloproteinase 2 with tissue inhibitor of metalloproteinase 2. *Proc. Natl. Acad. Sci. U.S.A.* **99,** 7414–7419 CrossRef Medline
67. Elliot, S., Catanuto, P., Stetler-Stevenson, W., and Cousins, S. W. (2006) Retinal pigment epithelium protection from oxidant-mediated loss of MMP-2 activation requires both MMP-14 and TIMP-2. *Invest. Ophthalmol. Vis. Sci.* **47,** 1696–1702 CrossRef Medline
68. Shen, Q., Lee, E. S., Pitts, R. L., Wu, M. H., and Yuan, S. Y. (2010) Tissue inhibitor of metalloproteinase-2 regulates matrix metalloproteinase-2-mediated endothelial barrier dysfunction and breast cancer cell transmigration through lung microvascular endothelial cells. *Mol. Cancer Res.* **8,** 939–951 Medline
69. Brooks, P. C., Silletti, S., von Schalscha, T. L., Friedlander, M., and Cheresh, D. A. (1998) Disruption of angiogenesis by PEX, a noncatalytic metalloproteinase fragment with integrin binding activity. *Cell* **92,** 391–400 CrossRef Medline
70. Boder, E. T., and Wittrup, K. D. (1997) Yeast surface display for screening combinatorial polypeptide libraries. *Nat. Biotechnol.* **15,** 553–557 CrossRef Medline
71. Colby, D. W., Kellogg, B. A., Graff, C. P., Yeung, Y. A., Swers, J. S., and Wittrup, K. D. (2004) Engineering antibody affinity by yeast surface display. *Methods Enzymol.* **388,** 348–358 CrossRef Medline
72. Boder, E. T., and Wittrup, K. D. (2000) Yeast surface display for directed evolution of protein expression, affinity, and stability. *Methods Enzymol.* **328,** 430–444 CrossRef Medline
73. Anderson, G. P., Glaven, R. H., Algar, W. R., Susumu, K., Stewart, M. H., Medintz, I. L., and Goldman, E. R. (2013) Single domain antibody–quantum dot conjugates for ricin detection by both fluoroimmunoassay and surface plasmon resonance. *Anal. Chim. Acta* **786,** 132–138 CrossRef Medline
74. Frankowski, H., Gu, Y.-H., Heo, J. H., Milner, R., and Del Zoppo, G. J. (2012) Use of gel zymography to examine matrix metalloproteinase (gelatinase) expression in brain tissue or in primary glial cultures. *Methods Mol. Biol.* **814,** 221–233 CrossRef Medline
75. Tamura, M., Gu, J., Takino, T., and Yamada, K. M. (1999) Tumor suppressor PTEN inhibition of cell invasion, migration, and growth: differential involvement of focal adhesion kinase and p130Cas. *Cancer Res.* **59,** 442–449 Medline
76. Brouet, A., Sonveaux, P., Dessy, C., Moniotte, S., Balligand, J. L., and Feron, O. (2001) Hsp90 and caveolin are key targets for the proangiogenic nitric oxide-mediated effects of statins. *Circ. Res.* **89,** 866–873 CrossRef Medline
77. Babae, N., Bourajjaj, M., Liu, Y., Van Beijnum, J. R., Cerisoli, F., Scaria, P. V., Verheul, M., Van Berkel, M. P., Pieters, E. H., Van Haastert, R. J., Yousefi, A., Mastrobattista, E., Storm, G., Berezikov, E., Cuppen, E., *et al.* (2014) Systemic miRNA-7 delivery inhibits tumor angiogenesis and growth in murine xenograft glioblastoma. *Oncotarget* **5,** 6687–6700 Medline
78. Husain, S. R., Joshi, B. H., and Puri, R. K. (2001) Interleukin-13 receptor as a unique target for anti-glioblastoma therapy. *Int. J. Cancer* **92,** 168–175 CrossRef Medline